



**HAL**  
open science

# Dynamics of molybdenum and barium in the Bay of Brest (France) explained by phytoplankton community structure and aggregation events

Valentin Siebert, Lukas Fröhlich, Julien Thébault, Bernd R Schöne, Gaspard Delebecq, Marc Picheral, Matthieu Waeles, Brivaëla Moriceau

## ► To cite this version:

Valentin Siebert, Lukas Fröhlich, Julien Thébault, Bernd R Schöne, Gaspard Delebecq, et al.. Dynamics of molybdenum and barium in the Bay of Brest (France) explained by phytoplankton community structure and aggregation events. *Estuarine, Coastal and Shelf Science*, 2024, 303, pp.108783. 10.1016/j.ecss.2024.108783 . hal-04573051

**HAL Id: hal-04573051**

**<https://hal.science/hal-04573051>**

Submitted on 13 May 2024

**HAL** is a multi-disciplinary open access archive for the deposit and dissemination of scientific research documents, whether they are published or not. The documents may come from teaching and research institutions in France or abroad, or from public or private research centers.

L'archive ouverte pluridisciplinaire **HAL**, est destinée au dépôt et à la diffusion de documents scientifiques de niveau recherche, publiés ou non, émanant des établissements d'enseignement et de recherche français ou étrangers, des laboratoires publics ou privés.



Distributed under a Creative Commons Attribution 4.0 International License



# Dynamics of molybdenum and barium in the Bay of Brest (France) explained by phytoplankton community structure and aggregation events

Valentin Siebert<sup>a</sup>, Lukas Fröhlich<sup>b</sup>, Julien Thébault<sup>a,\*</sup>, Bernd R. Schöne<sup>b</sup>, Gaspard Delebecq<sup>a</sup>, Marc Picheral<sup>c</sup>, Matthieu Waeles<sup>a</sup>, Brivaëla Moriceau<sup>a</sup>

<sup>a</sup> Univ Brest, CNRS, IRD, Ifremer, LEMAR, F29280, Plouzané, France

<sup>b</sup> Institute of Geosciences, University of Mainz, Johann-Joachim-Becher-Weg 21, 55128, Mainz, Germany

<sup>c</sup> Sorbonne Université, Centre National de la Recherche Scientifique, Laboratoire d'Océanographie de Villefranche (LOV), Villefranche-sur-Mer, France

## ARTICLE INFO

### Keywords:

Phytoplankton  
Biogeochemistry  
Aggregates  
Molybdenum  
Barium  
Benthic-pelagic coupling

## ABSTRACT

Primary producers are essential organisms for marine ecosystems because they form the basis of food webs, produce half of atmospheric oxygen and are involved in various biogeochemical cycles. At the end of a bloom event, phytoplankton cells are known to produce organic compounds that act as a 'cement', allowing the cells to stick together and form large sinking structures called aggregates. These aggregates are microenvironments with chemical properties that are very different from the surrounding water. The main objective of this study was to determine how the temporal variations in cell assemblages over time and the formation of aggregates following a bloom affect the concentrations of molybdenum (Mo) and barium (Ba) in the water column, which are elements typically measured within accretionary hard tissues (e.g., mollusc shells) to track phytoplankton dynamics in the environment. To do so, we performed an environmental monitoring from March to October 2021 at Lanvéoc in the Bay of Brest (France) during which several biological (e.g., variations in phytoplankton assemblages) and chemical (e.g., chemical properties of the water column) parameters were measured once to twice per week. Our results show that spring and summer blooms of *Gymnodinium*, known to be enriched in Mo, could be one of the reasons explaining the particulate Mo enrichments in the water column. In addition, large phytoplankton aggregates transported a significant amount of Mo to the seafloor and associated suspension feeders. In contrast, the temporal variations in dissolved and particulate Ba concentration were strongly influenced by the formation of diatom blooms. Interestingly, there was a significant shift in Ba from the dissolved to the particulate fraction during the largest diatom bloom in late spring, associated with a significant Ba transport to the seafloor, which may be explained by the adsorption of this element onto diatom frustules. This study therefore highlights the impacts of phytoplankton on the dynamics of these elements in coastal ecosystems.

## 1. Introduction

Marine phytoplankton are among the most important organisms of the biosphere. They are responsible for nearly half of the global primary production (Field et al., 1998). One fourth of this primary production occurs in coastal ecosystems (Boyce et al., 2010), although they represent only 2% of the earth surface (Charpy-Roubaud and Sourmia, 1990). Moreover, microalgae are at the base of the trophic network and are involved in several biogeochemical cycles. In light of the events caused by their seasonal development (bloom, appearance of harmful algae,

etc.), phytoplankton strongly modify the physical and chemical conditions of the water column on seasonal scales (Redfield, 1958) and these changes strongly affect organisms and ecosystems.

Naturally or under stressful conditions such as nutrient limitation due to a bloom event, high hydrodynamic energy or changes in temperature or light conditions, phytoplankton cells can excrete large amounts of extracellular polysaccharides (EPS) (Mykkestad, 1995). In particular, one form of EPS has been studied and is now well-documented: transparent exopolymer particles (TEPs) (e.g., Alldredge et al., 1993; Passow and Alldredge, 1994; Passow, 2002). The

\* Corresponding author.

E-mail addresses: [valentin.siebert@univ-brest.fr](mailto:valentin.siebert@univ-brest.fr) (V. Siebert), [lufroehl@uni-mainz.de](mailto:lufroehl@uni-mainz.de) (L. Fröhlich), [julien.thebault@univ-brest.fr](mailto:julien.thebault@univ-brest.fr) (J. Thébault), [bernd.schoene@uni-mainz.de](mailto:bernd.schoene@uni-mainz.de) (B.R. Schöne), [gaspard.delebecq@univ-brest.fr](mailto:gaspard.delebecq@univ-brest.fr) (G. Delebecq), [marc.picheral@imev-mer.fr](mailto:marc.picheral@imev-mer.fr) (M. Picheral), [matthieu.waeles@univ-brest.fr](mailto:matthieu.waeles@univ-brest.fr) (M. Waeles), [brivaela.moriceau@univ-brest.fr](mailto:brivaela.moriceau@univ-brest.fr) (B. Moriceau).

<https://doi.org/10.1016/j.ecss.2024.108783>

Received 4 April 2023; Received in revised form 4 April 2024; Accepted 26 April 2024

Available online 30 April 2024

0272-7714/© 2024 The Authors. Published by Elsevier Ltd. This is an open access article under the CC BY license (<http://creativecommons.org/licenses/by/4.0/>).

presence of TEPs in the water column appears to be essential for the formation of most phytoplankton aggregates, because they act as an organic ‘cement’ that will bind the cells together along with other inorganic particles of the environment (Passow and Alldredge, 1994; Dam and Drapeau, 1995; Logan et al., 1995). These so-called aggregates, also known as ‘marine snow’, can reach a few centimetres in diameter (Alldredge and Silver, 1988). Due to their fast sinking rates that average  $50 \text{ m d}^{-1}$  – but can reach several kilometers per day in the open ocean (Diercks and Asper, 1997; McDonnell et al., 2015; Toullec et al., 2021; Laurenceau-Cornec et al., 2020) – these aggregates have a major impact on ecosystems, being important vectors of organic matter export to the seafloor in shallow water as well as in the open ocean and also affect the biological carbon pump (Turner, 2015). These structures form ‘micro-environments’ that are highly porous and are known to transport not only particulate matter, but also dissolved elements after scavenging on these sinking particles (Carlson et al., 1994; De La Rocha et al., 2008; Moriceau et al., 2014).

Phytoplankton aggregates have their own internal chemical and biological dynamics that are quite different from those of the surrounding water (Alldredge et al., 1986; Alldredge and Cohen, 1987; Alldredge and Gotschalk, 1990; Kjørboe and Jackson, 2001; Garvey et al., 2007; Moriceau et al., 2007; Ploug et al., 2008). Several studies have recorded high heterotrophic activity and high phytoplankton cell viability within aggregates, which may explain their lower oxygen concentrations and pH values in comparison with surrounding water (Alldredge and Cohen, 1987). The combination of these factors, taken together with the high potential of the aggregate matrix to bind trace metals and other elements (Gutierrez et al., 2012; Tercier-Waeber et al., 2012), suggests that the elemental composition of the water mass can be modified when aggregates form and sink through the water layers. In particular, sinking aggregates may especially affect trace elements that are sensitive to redox conditions and ligand concentrations. Aggregate formation may therefore have a significant impact on the concentration of trace elements in water, as well as on their availability for living organisms and their transport toward the sediment/water interface (SWI).

Establishing the link between phytoplankton aggregate formation (or phytoplankton dynamics in general) and element composition of seawater remains an important challenge. Over the past two decades, attempts have been made to identify links between trace elements, specifically molybdenum (Mo) and barium (Ba), incorporated into the shells of bivalves and changes in micro-algae communities (e.g. Vander Putten et al., 2000; Barats et al., 2009; Thébault et al., 2009; Tabouret et al., 2012; Doré et al., 2021; Thébault et al., 2022; Fröhlich et al., 2022a). This field is known as bivalve sclerochronology and aims to reconstruct past phytoplankton dynamics from times prior to major anthropogenic impacts on coastal ecosystems as well as times and places for which instrumental records of phytoplankton abundance are not available. For example, Mo enrichments recorded into bivalve hard and soft tissues have already been observed in the periostracum of *Mytilus edulis* (Kowalski et al., 2013) and in the carbonate shell of *Pecten maximus* (Thébault et al., 2022). These enrichments have been attributed to the sinking of organic matter such as Mo-rich aggregates (e.g., Thébault et al., 2022), or *Phaeocystis* sp. blooms (Kowalski et al., 2013), which can contribute to a significant Mo transport toward the seabed (Dellwig et al., 2007; Kowalski et al., 2013). Moreover, previous studies highlighted that Ba incorporated in higher rate into scallop shells could be an indicator of a higher amount of phytoplankton cells in the water column, and especially diatoms (Fröhlich et al., 2022b), since Ba can be adsorbed on their frustules (Dehairs et al., 1980; Fisher et al., 1991; Sternberg et al., 2005). However, to be considered as proxies for phytoplankton dynamics or for the presence of aggregates in the water column, it is necessary to understand how variations in phytoplankton assemblage and the formation of aggregates impact the availability of Mo and Ba for suspension feeders, as well as their transport toward the seafloor, which are still poorly known. Furthermore, it is crucial to differentiate these processes from other important scavenging mechanisms on other types

of particles, such as the scavenging of Mo on Mn oxides (Berrang and Grill, 1974) or the partitioning of Ba through the formation of barite crystals (Dehairs et al., 1980).

The specific objective of this paper is to assess potential links between phytoplankton dynamics (temporal variations in micro-algae assemblages, aggregate formation) and Mo and Ba concentrations in the Bay of Brest. We explored the processes related to phytoplankton dynamics that control the distribution of these elements between the particulate and dissolved compartments and their transport to the SWI during the productive season. This study will therefore provide new insights into the behaviour of these elements with regard to phytoplankton and aggregation dynamics, enabling future sclerochronological studies using these elements to refine their hypotheses.

## 2. Material and methods

### 2.1. Study site

The Bay of Brest, France, is a semi-enclosed, macrotidal marine ecosystem of  $180 \text{ km}^2$  with a connection to the Iroise Sea to the west, separated by a narrow (2 km width) and deep strait (40 m max. depth) (Fig. 1). Freshwater input occurs from the east via two main rivers: the Aulne flows from the south and the Elorn from the north of the bay. The present study was carried out in 2021 and took place at Lanvéoc ( $48^{\circ}17'39''\text{N}$ ,  $004^{\circ}27'12''\text{W}$ ), a site located in the southern part of the Bay of Brest (Fig. 1). This site was chosen because several ecological and sclerochronological studies have already been conducted at this locality, making it possible to compare our new data with those from the past 10 years (e.g., Fröhlich et al., 2022a, 2022b; Thébault et al., 2022). Lanvéoc is characterized by shallow (6–13 m depending on tides, with a mean depth of approx. 10 m at mid-tide) and well-mixed waters, with a salinity ranging from 32 to 35. The study site is also characterized with a seafloor consisting of sandy and silty sediment.

### 2.2. Environmental monitoring

The study covered seven months of the year 2021 during which several chemical, physical and biological parameters were recorded at Lanvéoc. From 16 March to 14 October 2021, water samples were collected by SCUBA diving in surface (1 m depth) and bottom waters (approx. 20 cm above the sediment) using two different types of sampling bottles placed horizontally in the water column. Due to the high sampling frequency (twice per week), samples were not collected under the same tidal conditions. Firstly, two 5-L Niskin bottles (one for surface water and the other for bottom water) were used to collect seawater dedicated to measurements of nutrients, particulate organic carbon (POC), chlorophyll *a* (Chl) and pheophytin *a* (Pheo; degraded form of the Chl) as well as nano- and micro-phytoplankton (cell size  $>5 \mu\text{m}$ ) species determination and cell counts. Analyses of these latter parameters were performed following protocols given in Siebert et al. (2023). Analytical precisions (expressed as relative standard deviations) were below 5% for each of them. On some days, bottom water samples were collected with a benthic syringe, which was positioned closer to the sediment than the Niskin bottle. Secondly, two 5-L GO-Flo, Teflon coated, water samplers were used in the same manner to collect water to measure particulate and dissolved trace elements. After collection, 2-L PTFE bottles were filled until further filtration at the home lab. These PTFE bottles were used to prevent the adsorption of elements on the bottle walls. In parallel, two NKE/Sambat probes positioned on the seafloor continuously recorded dissolved oxygen (DO) concentration and salinity every 20-min.

Besides, a HYDRO-BIOS Multi Sediment Trap with 12 collecting bottles was installed on the seafloor to trap sinking particles, allowing us to measure their chemical composition. It was equipped with a cylindrical sampling body with a catchment area of  $154 \text{ cm}^2$  and an entrance situated 1 m above the seafloor. The rotation frequency was set to one

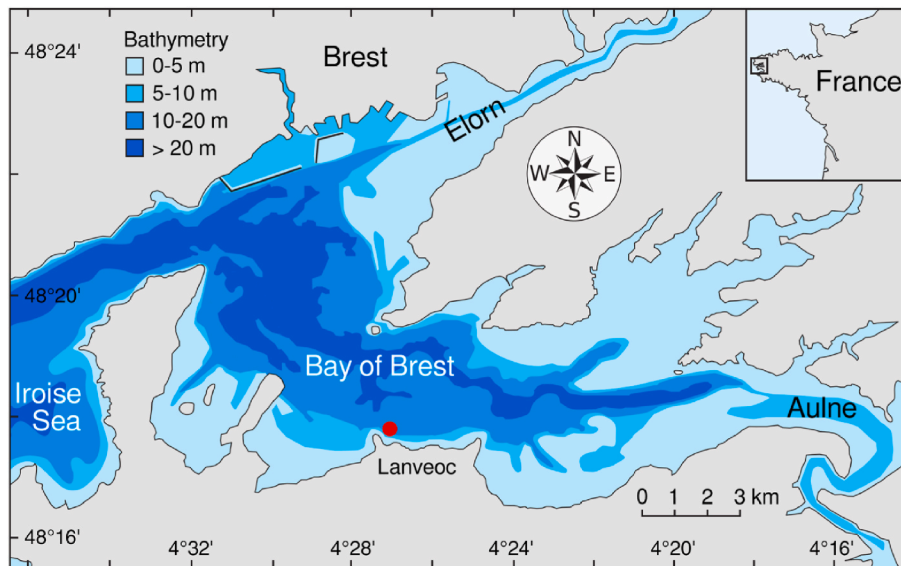


**Fig. 1.** Locality of the study site (Lanvéoc: red filled circle) (modified after Thébault et al., 2022). (single column). (For interpretation of the references to colour in this figure legend, the reader is referred to the Web version of this article.)

every three days between 2 March and 25 May, and one every four days between 26 May and 29 July. Before installation, each bottle was poisoned with mercury chloride ( $180 \mu\text{M HgCl}_2$ , Lee et al., 1992) to prevent any biological activity and thus the degradation of organic matter. Parameters to be measured from this material included the fluxes of particulate Mo and Ba, POC and biogenic silica (BSi) following the methods described in following sections or in Siebert et al. (2023). All fluxes are expressed in  $\text{mmol h}^{-1} \text{m}^{-2}$ . Prior to filtration, samples were shaken to break up aggregates and passed through a 1-mm mesh screen to avoid heterogeneity due to large mineral particles or zooplankton.

Finally, aggregate dynamics was measured throughout the year by using a compact and autonomous underwater imaging system initially constructed and developed at the Laboratoire d’Oceanographie de Villefranche-sur-Mer (LOV – France), i.e., the Underwater Vision Profiler 6 (UVP6) (see Picheral et al. (2021) for a complete description of the instrument). The device consists of a camera coupled to a light source that can take pictures of particles in a precisely defined volume of water (0.65 L) at a pre-defined frequency (Fig. 2A). This instrument was designed for intermittent profile measurements, but we used it to measure particle dynamics as a continuous time-series; we thus modified the design of the UVP6 accordingly. Several environmental parameters may have influenced measurements and biased the results, such as sun exposure, bioturbation, particle resuspension from the sediment and hydrodynamic conditions. To limit these potential biases, the UVP6 was placed in a PVC cylinder (diameter = 50 cm; height = 70 cm) which was open at the top and closed at the bottom. To prevent large organisms

from entering the cylinder and to ensure that constant hydrodynamics prevailed within the cylinder, a 5-cm thick grid with a  $1 \times 1 \text{ cm}$  mesh size was placed on top of the cylinder (Fig. 2B). The UVP6 was installed on the seafloor at Lanvéoc on 16 March 2021. Data acquisition took place every hour for 30 min. During that time, the UVP6 took pictures of particles every 20 s. With the chosen settings, the UVP6 worked autonomously for approx. 21 days. Every 3 weeks, the UVP was recovered, data were downloaded and the batteries were recharged. The pictures were later processed using the UVP application, which can automatically detect particles on pictures, count them and measure their size in equivalent spherical diameters (ESD - Jennings and Parslow, 1988). However, measurements acquired 1 h before and 2 h after each cruise were removed to prevent potential bias induced by the divers (e.g., particle resuspension). After processing, the database contained measurements of particle concentration divided into 25 particle size classes ranging from  $80.6 \mu\text{m}$  to 26 mm (ESD).

Table 1 gives an exhaustive list of all parameters that were measured and used for this study.

### 2.3. Mo and Ba analysis

Samples collected with GO-Flo bottles for the water column and with sediment trap for sinking material were filtered through  $0.45 \mu\text{m}$  MF-Millipore™ mixed cellulose ester filters within 3 h after collection. Filters were then rinsed with ultra-pure (UP) water from a Milli-Q element system, air-dried and stored in a dark and dry place to measure the trace elements in the particulate fraction. The filtered water, dedicated to

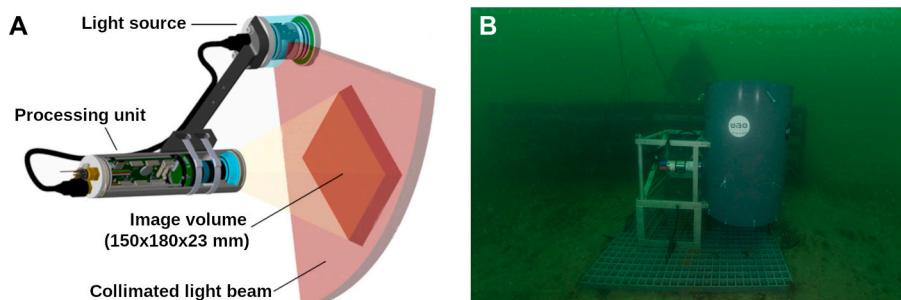


**Fig. 2.** (A) Expanded view of the UVP6 showing the main features of the instrument (modified after Picheral et al., 2021). (B) Picture of the UVP6 deployed at Lanvéoc showing the modifications made to adapt the UVP deployment for continuous measurements in a coastal ecosystem. (two columns).

**Table 1**  
Summary of the parameters that were measured and used during the survey. (two columns).

Parameter	Date of first acquisition	Date of last acquisition	Frequency	Surface/bottom water	Sampling method
Salinity	01 January 2021	31 December 2021	Every 20 min	Bottom water	Sambat probes
Dissolved oxygen (DO)	01 January 2021	31 December 2021	Every 20 min	Bottom water	Sambat probes
Nutrients	16 March 2021	14 October 2021	- Twice per week (from 16 March to 28 June) - Once per week (from 05 July to 14 October)	Surface water	SCUBA diving Niskin bottle
Biogenic silica (BSi)	16 March 2021	14 October 2021	- Twice per week (from 16 March to 28 June) - Once per week (from 05 July to 14 October)	Sediment trap	
Chlorophyll <i>a</i> (Chl) and pheophytin (Pheo)	16 March 2021	14 October 2021	- Twice per week (from 16 March to 28 June) - Once per week (from 05 July to 14 October)	Surface water Bottom water	SCUBA diving Niskin bottle
Particulate organic carbon (POC)	16 March 2021	14 October 2021	- Twice per week (from 16 March to 28 June) - Once per week (from 05 July to 14 October)	Surface water Bottom water Sediment trap	SCUBA diving Niskin bottle
Phytoplankton determination and counts	07 January 2021	13 December 2021	Every second week	Surface water	SCUBA diving Niskin bottle
Particulate <sup>95</sup> Mo (PMo) and <sup>138</sup> Ba (PBa) concentrations	16 March 2021	14 October 2021	- Twice per week (from 16 March to 28 June) - Once per week (from 05 July to 14 October)	Surface water Bottom water Sediment trap	SCUBA diving GO-Flo bottle
Dissolved <sup>95</sup> Mo (DMo) and <sup>138</sup> Ba (DBa) concentrations	16 March 2021	14 October 2021	- Twice per week (from 16 March to 28 June) - Once per week (from 05 July to 14 October)	Surface water Bottom water Sediment trap	SCUBA diving GO-Flo bottle
Size-dependent particle concentration	16 March 2021	14 October 2021	Every hour	Bottom water	UVP6

trace element analyses in the dissolved phase, was stored in 15-mL polypropylene (PP) tubes at 4 °C. The filters and PP tubes were pre-washed by soaking them for at least 24 h in a pH~1 solution made by diluting concentrated nitric acid (HNO<sub>3</sub>, Suprapur 65%, Merck, Darmstadt, Germany) with UP water by a factor 100. The filters were then soaked in UP and thoroughly rinsed with UP before use.

**Trace element analysis of particulate matter** – For the analysis of particulate <sup>95</sup>Mo (PMo) and particulate <sup>138</sup>Ba (PBa) in the water column and in sediment trap samples, the filters were rinsed with UP water after filtration and digested at 80 °C for 3 h in closed 30-mL PTFE screw-cap vials (Savillex, Minnetonka, MN, USA) by adding 2 mL of 65% HNO<sub>3</sub> (Suprapur, Merck) and 500 µL of 30% hydrogen peroxide (Suprapur, Merck). The elemental analyses of <sup>95</sup>Mo and <sup>138</sup>Ba isotopes were then conducted on diluted mixtures (2.3% HNO<sub>3</sub>, dilution factor = approx. 25) with a X-series II, quadrupole inductively coupled plasma mass spectrometer (Q-ICP-MS) (Thermo Scientific) equipped with a H<sub>2</sub> collision cell at the Pôle Spectrométrie Océan (Plouzané, France). The data were corrected for instrument drift by inserting multi-element standard solutions every two samples. The procedural blanks were determined after digestion of cleaned filters and analyses of the resulting solutions. The obtained values were 0.029 nmol for Mo and 0.026 nmol for Ba. Only values significantly above the procedural blank were interpreted. All PBa data and 76% of the PMo data significantly exceeded the procedural blank. Measurements were conducted with a precision (relative standard deviation) of 2.9% for Mo and 1.7% for Ba. To detect PMo and PBa enrichment episodes in the organic matter of the water column, results will be given as ratios of these elements relative to POC concentration (PMo:POC and PBa:POC, respectively).

**Trace element analysis of dissolved matter** – Dissolved <sup>95</sup>Mo (DMo) and <sup>138</sup>Ba (DBa) concentrations were measured in low resolution using an Element XR HR-ICP-MS at IFREMER (Plouzané – France). Seawater samples were diluted 100 times with 2% HNO<sub>3</sub> solutions in order to preserve the instrument from the salt matrix. The drift of the instrument was also taken into account and the data were corrected accordingly using indium (In) as an internal standard. The accuracy of the method was verified using a NASS-6 (National Research Council, Canada)

certified reference seawater (precision of 1.87 % and 2.02 % for Mo and Ba, respectively). Note that no certified values are provided for Ba in the initial certificate of the NASS-6 standard material. We thus used the indicative Ba value provided by GeoReM (<http://georem.mpch-mainz.gwdg.de/>; last access: 7 November 2023). LOD values were 0.04 nM and 0.01 nM for DMo and DBa, respectively, and 100% of the data exceeded these LODs. DMo deficit was quantified, at a given salinity (salinity measured at our study site was in the range of approx. 32–35 – Siebert et al., 2023), by difference between (i) the expected value for a conservative mixing between the Aulne River end-member (DMo = 1 nM) (Waeles et al., 2013) and the oceanic end-member (DMo = 107 nM, Morris, 1975) and (ii) the measured DMo concentration.

#### 2.4. Aggregate dynamics and particle abundance

Based on the data produced by the UVP, a first overview of aggregate dynamics was obtained by calculating the sum of particles larger than 512 µm (ESD). We thus avoided including large phytoplankton cells that can reach this size; for example, cells of *Coscinodiscus* spp. (among the largest phytoplankton species) can have a cell diameter of up to 500 µm (Kühn and Raven, 2008). We also excluded particles larger than 26 mm to avoid counting debris or macroparticles other than organic aggregates. Following these rules, an event was considered as an aggregation episode when the maximum value (peak) of the particle concentration exceeded the width of its base peak by two-fold.

To better characterize the aggregation episodes, particle size spectra were obtained by computing the concentration of particles as a function of their size range on each day of monitoring, as previously done for aggregates artificially produced in rolling tanks (Laurenceau-Cornec et al., 2015). For each spectrum, the slope of the linear regression between particle size and concentration was then calculated, providing information on a potential transition between small and large particles, and therefore, on the occurrence of an aggregation event. For instance, higher slope values (closer to 0 since slopes are negative) indicate that a high number of small particles have agglomerated with each other to form larger particles. This indicates the presence of large aggregates

occurring at high concentrations, thereby revealing an aggregation event. Combined with the previous method, these daily measurements of aggregate dynamics were very useful because they identified other aggregation episodes that were composed of larger particles, likely otherwise undetectable due to their very low concentrations. For every detected aggregation event based on these two methods, their slopes were compared using an analysis of covariance (ANCOVA) to observe differences in the structure of the aggregation episodes.

### 3. Results

#### 3.1. Nutrients

At Lanvéoc in 2021, all macronutrients followed more or less the same general trend (Fig. 3). The maximum concentrations were observed during winter, followed by a rapid decrease to low concentrations in mid-spring. Concentrations remained low until mid-summer before they gradually increased until the end of the monitoring survey (Fig. 3A). Episodes of nutrient limitation were defined by comparing in situ concentrations to the half-saturation constant for nutrient uptake ( $K_m$ ). Values below this threshold correspond to stressful nutrient conditions limiting phytoplankton development ( $K_m = 2.0 \mu\text{mol L}^{-1}$  for DIN and  $\text{Si(OH)}_4$ ;  $K_m = 0.2 \mu\text{mol L}^{-1}$  for  $\text{PO}_4^{3-}$ ; Del Amo et al., 1997).  $\text{PO}_4^{3-}$  was the first limiting nutrient with concentrations below the  $K_m$  value between the end of March and late summer. DIN was physiologically limiting a few weeks after  $\text{PO}_4^{3-}$ , between mid-April and late summer, i. e., when concentrations began to rise.  $\text{NO}_3^-$  constituted most of the DIN (80% throughout the year; Fig. 3B), but all three nitrogen co-products showed the same trends. Silicic acid had the shortest limitation period

(from early April to mid June), which was interrupted by a low enrichment at the end of May, before becoming limiting again from early to mid-June.

#### 3.2. Properties of particulate organic matter

Fig. 4 presents Chl:Pheo and POC:Chl ratios in surface and bottom

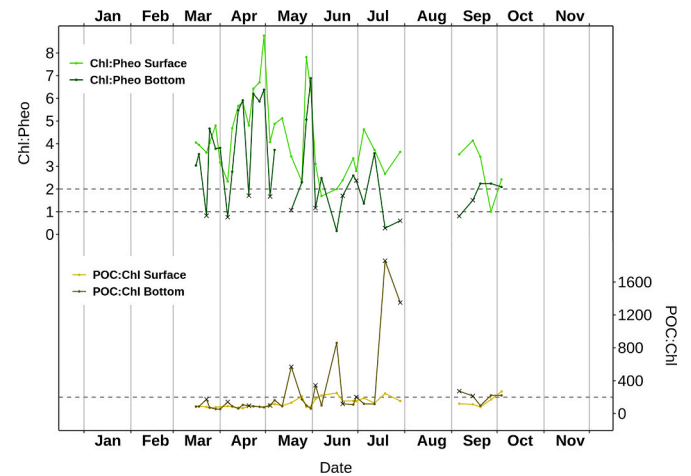


Fig. 4. Chl:Pheo and POC:Chl ratios measured at Lanvéoc in bottom and in surface waters. Horizontal dashed grey lines represent the threshold values indicated in the text for the Chl:Pheo and POC:Chl ratios. (single column).

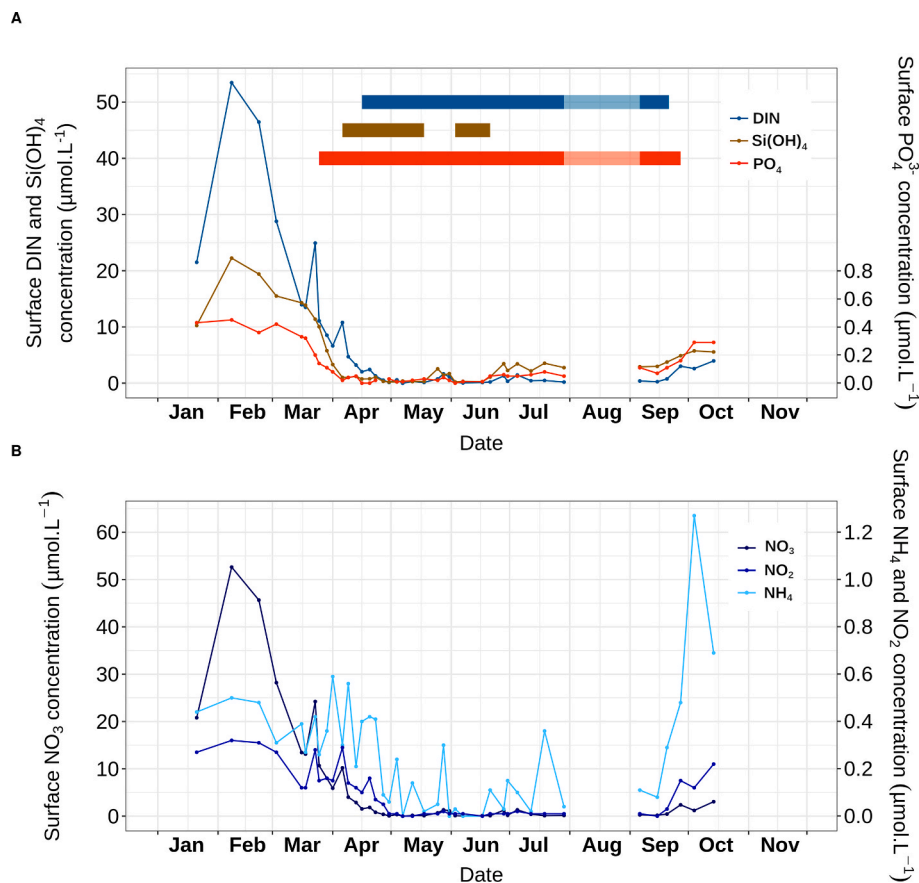


Fig. 3. (A) Dissolved inorganic nitrogen (DIN – blue line), silicic acid (brown line), phosphate (red line) concentrations with their respective periods of limitation (thick solid lines – transparent portions indicate the time interval when no cruise was conducted). (B) Nitrate, nitrite and ammonium concentrations recorded at Lanvéoc in 2021. (single column). (For interpretation of the references to colour in this figure legend, the reader is referred to the Web version of this article.)

waters. Chl:Pheo (expressed in  $\text{g g}^{-1}$ ) gives information on the degree of phytoplankton degradation. According to Savoye (2001), a value below 1 indicates degraded organic matter and a value greater than 2 describes fresh phytoplankton. At Lanvéoc in 2021, Chl:Pheo ratios were almost entirely greater than 2 in the surface layer, suggesting active phytoplankton growth with the exception of two time intervals: early June (1.69) and late September (1.00) (Fig. 4). In the bottom layer, this ratio occasionally fell below 1, e.g., in late March (0.82) and early April (0.76). Moreover, a Chl:Pheo ratio close to 1 was also recorded in early June in the bottom layer (1.16), and a minimum of 0.15 was recorded a few days later, on mid-June. With the exception of the minimum value recorded on mid-June, it is important to note that all these low values in the bottom water were obtained on samples collected with a benthic syringe, thus closer to the sediment than with the Niskin bottle.

POC:Chl ratio (expressed in  $\text{g g}^{-1}$ ) provides information on photosynthesis efficiency: values greater than 200 are used as a threshold to detect time intervals during which the efficiency of photosynthesis is reduced, and mixotrophy and heterotrophy dominate (Bentaleb et al., 1998). In surface water, the POC:Chl ratio remained relatively constant throughout 2021, with values oscillating between 65 and 251 (Fig. 4). However, values barely never exceeded the threshold of 200. The POC:Chl signals in bottom water roughly mirrored those recorded in the surface layer, with the same low values (fluctuating between 55 and 173) interrupted by episodic sharp peaks. These peaks were much higher and significantly exceeded 200 in mid-May (570), early June (344), mid-July (1860) and late July (1351) (Fig. 4). As for Chl:Pheo, it is noteworthy that all the cited time intervals corresponded to a high POC:Chl ratio in water samples collected with a benthic syringe, with the exception of mid-July, when the bottom seawater sample was collected with a Niskin bottle.

The POC signal obtained throughout the year with the sediment trap showed episodes of low and high fluxes of organic carbon toward the SWI (Fig. 5). In total, five main episodes of high carbon flux were detected. The first occurred in late March ( $5.7 \text{ mmol h}^{-1} \text{ m}^{-2}$ ), the second in late April ( $3.7 \text{ mmol h}^{-1} \text{ m}^{-2}$ ), the third in late May ( $4.6 \text{ mmol h}^{-1} \text{ m}^{-2}$ ), the fourth in mid-June ( $1.9 \text{ mmol h}^{-1} \text{ m}^{-2}$ ) and the fifth in late June ( $5.0 \text{ mmol h}^{-1} \text{ m}^{-2}$ ). Fig. 5 also shows the BSi:POC signal recorded in the sediment trap samples. This ratio (expressed in  $\text{mol}^{-1}$ )

is representative of phytoplankton composition since more than 88% of diatom species have a Si:C signature between 0.05 and 0.19 (average = 0.14) (Sarhou et al., 2005). In our study site, it oscillated between  $0.01 \text{ mol mol}^{-1}$  and  $0.44 \text{ mol mol}^{-1}$  and was quite variable throughout the year. As explained above, this ratio can be used to detect whether the sedimented organic matter reflects the presence of diatoms. Two time intervals of significant diatom sedimentation were identified (with BSi:POC values close to 0.14). The first occurred between early and mid-May, with a BSi:POC values ranging between 0.12 and 0.18, the second one between early and late June, with a ratio varying between 0.09 and 0.16 (Fig. 5).

### 3.3. Phytoplankton and aggregates dynamics

Every fortnight, surface seawater was sampled at Lanvéoc to monitor the development of the phytoplankton community throughout the year. Three main events can be noticed in the annual phytoplankton dynamics (Fig. 6A). While minimal cell counts occurred at the beginning of the year (approx.  $100,000 \text{ cells L}^{-1}$ ), a small elevation appeared in mid/late April ( $340,980 \text{ cells L}^{-1}$ ) before values slightly dropped close to the baseline value in mid-May (Fig. 6A). The main phytoplankton bloom occurred a few days later in early June ( $2,258,580 \text{ cells L}^{-1}$ ) and a second important bloom was detected in mid-September ( $1,516,940 \text{ cells L}^{-1}$ ) (Fig. 6A). Throughout the year, the phytoplankton community was mostly composed of diatoms (88%), with dinoflagellates (4%) and other taxa (e.g., Cryptophyceae and Chrysophyceae; 8%) accounting for the remaining minority.

Through the calculation of the biovolumes of certain cells, it was possible to detect five dominant diatom species that occurred successively and formed a total of six significant blooms: *Coscinodiscus wailesii* (mid/late March), *Cerataulina pelagica* (mid/late April), *Guinardia* spp. (mid-May), *Leptocylindrus danicus* (early June and mid-September) and *Chaetoceros* spp. (mid-June) (Fig. 6B). On the other side, dinoflagellate species were mainly represented by three species, namely *Gymnodinium* spp. which bloomed thrice (late April, mid-June and mid-September), *Protoperidinium* spp. (early June) and *Prorocentrum triestinum* (mid-September) (Fig. 6C).

The daily mean concentration of particles above  $512 \mu\text{m}$  (ESD) at Lanvéoc showed a succession of high and low values, with a minimum concentration of  $4.9 \text{ part L}^{-1}$  (23 March) and a maximum value of  $151 \text{ part L}^{-1}$  (30 March) (Fig. 7A). Four aggregation periods occurred, with maximum particle concentration value exceeding by more than two-fold the value at the base of each peak (vertical grey intervals on Fig. 7A and B). The first and highest peak was observed on 30 March ( $151 \text{ part L}^{-1}$ ), the second on 27 April ( $128 \text{ part L}^{-1}$ ), the third on 13 May ( $78 \text{ part L}^{-1}$ ) and the fourth on 6 June ( $113 \text{ part L}^{-1}$ ).

From the slope of the regression line between daily particle size and concentration, four additional aggregation episodes were detected (red vertical areas on Fig. 7A and B). It is noteworthy that each of the four periods detected above corresponded to a peak or at least a change in the slope of the regression lines. These four new aggregation events occurred on 12 April, 14 June, 26 June and 2 October 2021 (Fig. 7B). Even if the concentration of particles above  $512 \mu\text{m}$  remained relatively low on these dates, the concentrations of large particles were high relative to the concentration of smaller particles. Fig. 7C shows the particle size spectra obtained for the eight days during which aggregation events were detected, offering a better picture of the aggregate structure on these dates. The slopes of these eight spectra were then compared pairwise using ANCOVA. Accordingly, three aggregation episode groups can be distinguished: one including the dates of 30 March, 12 April and 13 May; another with the dates of 14 June, 27 June and 2 October; and a last group with the dates of 6 June and 27 April. The slopes recorded on 30 March, 12 April and 13 May were significantly lower than those obtained on 14 June, 27 June and 2 October. This indicates that the aggregation events that occurred on 30 March, 12 April and 13 May were characterized by aggregates that were

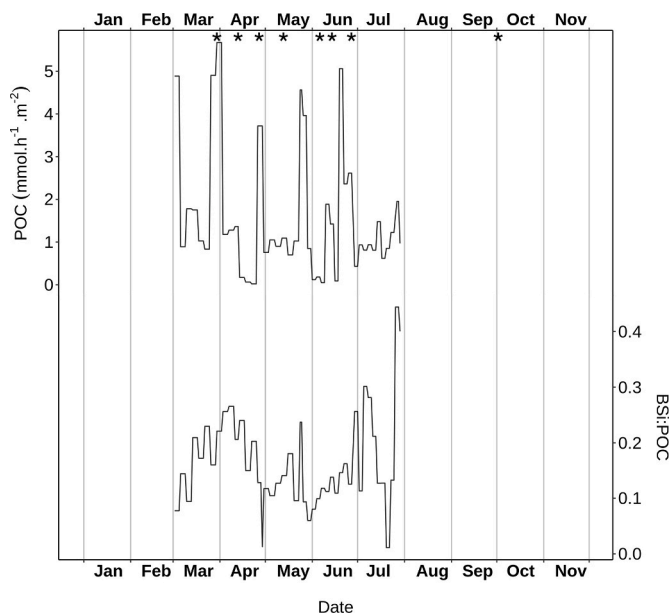
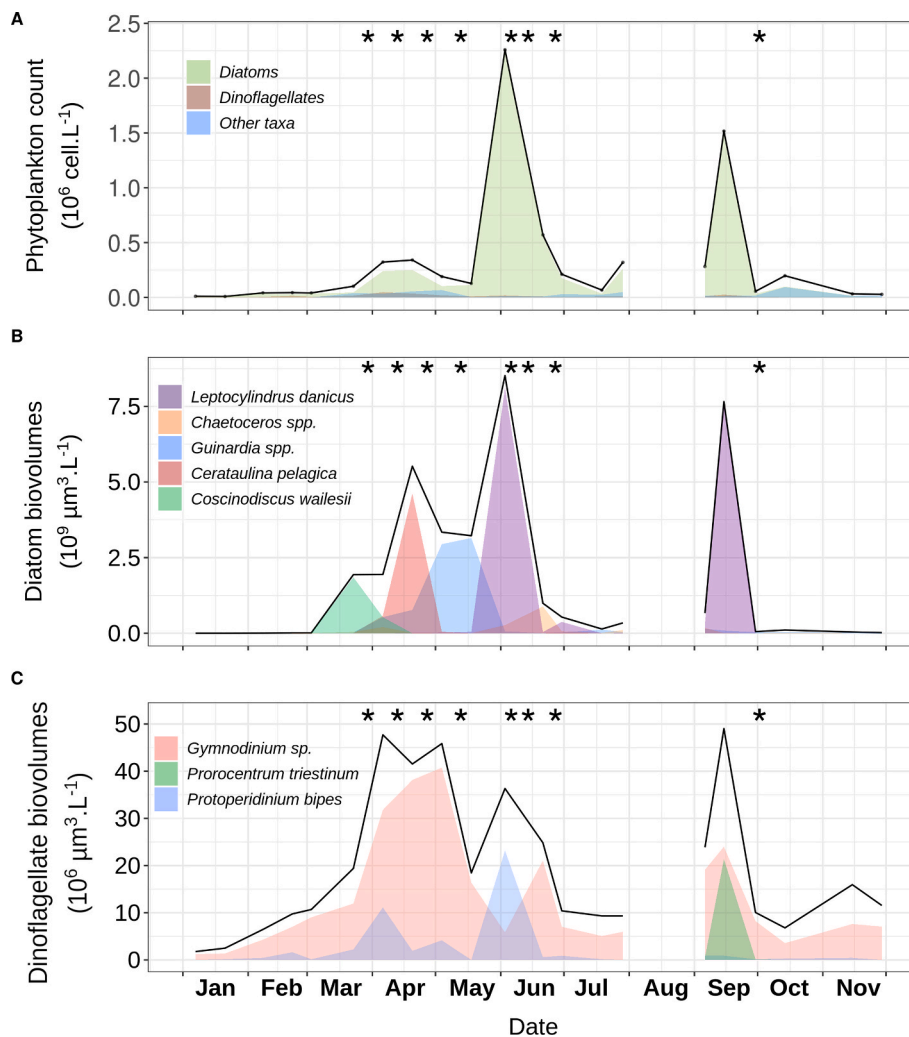


Fig. 5. POC concentration (upper panel) and BSi:POC ratio (lower panel) measured in the sediment trap samples at Lanvéoc in 2021. Black asterisks indicate the aggregation episodes that were defined in Section 3.3. (single column).



**Fig. 6.** (A) Phytoplankton dynamics recorded at Lanvéoc in 2021. Relative presence of the main diatoms (B) and the main dinoflagellate species (C) expressed as cell biovolumes. Black asterisks represent the eight aggregation events that were defined in Section 3.3. (*two columns*).

significantly smaller than those observed on 14 June, 27 June and 2 October, which showed the largest aggregates. Finally, aggregation events of 27 April and 6 June had an intermediate status and were highly similar to all other events. Therefore, they were either mainly composed by aggregates of intermediate size or evenly distributed aggregate sizes.

### 3.4. Dissolved and particulate trace element concentrations

#### 3.4.1. Molybdenum

The concentration of  $\text{DMo}_{\text{norm}}$  remained relatively stable, with values generally oscillating in the range 70–80 nM in surface and bottom waters, of which signals are significantly similar based on Spearman's rank correlation ( $\rho = 0.50$ ,  $p < 0.01$ ) (Fig. 8A). However, two slight decreases in  $\text{DMo}_{\text{norm}}$  were observed in late April and late June, with values dropping from 76.2/76.9 nM to 63.2/65.2 nM in late April and from 75.9/77.4 nM to 68.1/69.7 nM in late June in bottom/surface waters (Fig. 8A). In parallel, three PMo:POC increases can be observed in surface and bottom water (Fig. 8B). In bottom water, PMo:POC ratios reached maxima in late April ( $59.6 \mu\text{mol mol}^{-1}$ ), late June ( $12.4 \mu\text{mol mol}^{-1}$ ) and mid-September ( $12.4 \mu\text{mol mol}^{-1}$ ). In surface waters, PMo:POC ratios followed the same trend as near the seafloor since PMo:POC profiles between surface and bottom water did not differ significantly ( $\rho = 0.81$ ,  $p < 0.001$ ) (Fig. 8B). To detect episodes of Mo enrichment in sinking particles, the PMo:POC<sub>trap</sub> ratio was also calculated from the sediment trap samples (Fig. 8C). The single large PMo:POC<sub>trap</sub> increase

observed in early June was uncoupled from the high PMo:POC peaks measured in the water column. This main PMo:POC<sub>trap</sub> increase lasted 27 days (from late May to late June) and reached a maximum of  $51.8 \mu\text{mol mol}^{-1}$  (Fig. 8C). Besides, three smaller increases were observed on the PMo:POC<sub>trap</sub> profile, one occurring in late April ( $16.2 \mu\text{mol mol}^{-1}$ ), another in mid-May ( $16.7 \mu\text{mol mol}^{-1}$ ) and finally one in late June ( $21.9 \mu\text{mol mol}^{-1}$ ) (Fig. 8C).

Fig. 8D and E also present parameters that could affect the behaviour of Mo in the environment. Fig. 8D presents the *Gymnodinium spp.* dynamics in the water column in cell count, which follow the same trends as presented in Fig. 6C (biovolumes). Besides, Fig. 8E presents the dissolved oxygen (DO) concentrations close to the SWI. DO concentrations oscillated between 7.8 and 10.9  $\text{mg L}^{-1}$ . Between January ( $8.1 \text{ mg L}^{-1}$ ) and mid-April ( $10.9 \text{ mg L}^{-1}$ ), a progressive increase in DO was detected and a short depletion was then recorded in late April ( $9.8 \text{ mg L}^{-1}$ ) before values rose up again until early May ( $10.7 \text{ mg L}^{-1}$ ) (Fig. 8E). A decrease in DO values was observed until late May ( $8.8 \text{ mg L}^{-1}$ ) and DO concentrations were then relatively stable until the end of the survey, with values ranging from 8.6 to 9.2  $\text{mg L}^{-1}$  (Fig. 8E).

#### 3.4.2. Barium

DBa concentrations exhibited values which ranged from 133 to 304 nM. Trends were similar between surface and bottom water and similar to  $\text{DMo}_{\text{norm}}$ , and no significant difference was found between DBa profiles between surface and bottom water ( $\rho = 0.83$ ,  $p < 0.001$ )

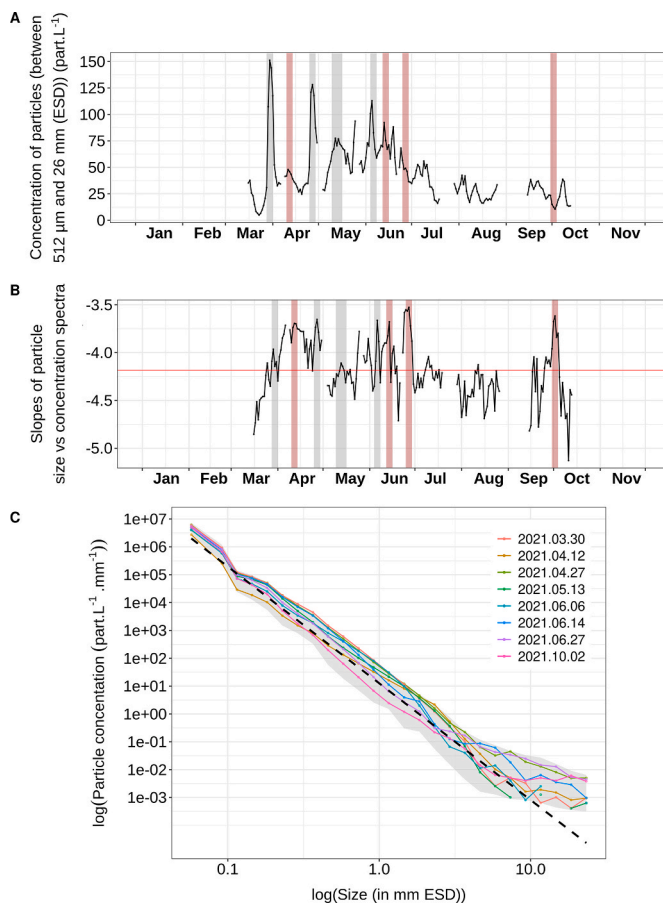


**Fig. 7.** (A) Average daily concentration of particles  $>512 \mu\text{m}$  recorded at Lanvéoc with the UVP6. (B) Slope of the daily size spectra of particles (black line) with the annually averaged slope value (horizontal red line). Vertical grey intervals represent the four aggregation events that were detected by calculating the sum of particle concentrations larger than  $512 \mu\text{m}$ , while the vertical red areas correspond to the four aggregation events that were detected with the size spectra method. (C) Size spectra of the eight dates when aggregation episodes were observed. Dashed black line represents the average slope of daily size spectra. (two columns). (For interpretation of the references to colour in this figure legend, the reader is referred to the Web version of this article.)

(Fig. 9A). A gradual decline in DBa was observed between mid-March ( $304/272 \text{ nM}$ ) and late May ( $231/230 \text{ nM}$ ) in bottom/surface waters. Then, a sharp depletion was observed in early June with minimum values of  $155/133 \text{ nM}$  in bottom/surface water (Fig. 9A). After this event in mid-June, the DBa values rose up to  $220/238 \text{ nM}$  and remained relatively constant (between  $200$  and  $260 \text{ nM}$ ) until the end of the survey; Fig. 9A). In parallel, seven PBa:POC peaks were observed in surface but the main ones occurred in early September ( $1130 \mu\text{mol mol}^{-1}$ ) and early June ( $404 \mu\text{mol mol}^{-1}$ ) (Fig. 9B). The latter coincided with the main DBa depletion (Fig. 9A). However, contrary to PMo:POC profiles, bottom PBa:POC did not exhibit the same number of enrichment periods than in surface, which is reflected in a lower, but still significant Spearman's correlation ( $\rho = 0.63$ ,  $p < 0.001$ ). In bottom water, four enrichments were recorded, with the main one occurring in early June ( $918 \mu\text{mol mol}^{-1}$ ) (Fig. 9B). In sediment trap samples, the PBa:POC<sub>trap</sub> values oscillated between  $1$  and  $132 \mu\text{mol mol}^{-1}$  until late May (Fig. 9C). Afterwards, one large PBa:POC<sub>trap</sub> increase was recorded between late May and mid-June ( $437 \mu\text{mol mol}^{-1}$ ) (Fig. 9C), indicative of a strong Ba transport event that occurred contemporaneously to the main PBa:POC peak recorded in the water column (Fig. 9B).

Because Ba was assumed to be linked with diatom cells, Fig. 9D presents the diatom dynamics expressed as cell counts, which can be

useful to detect bloom composed with small cells, in opposition to results presented in Fig. 6B that were based on cell biovolumes. However, the observed dynamics remained similar as described above, with the occurrence of the same species with the exception of *Co. wailesii*. Moreover, a new small and important species (*Tenuicylindrus belgicus*), for which biovolume data were not available in our database, formed a bloom simultaneously with *L. danicus* in early June (Fig. 9D).

## 4. Discussion

### 4.1. Phytoplankton dynamics: triggers of aggregation episodes

To our knowledge, this is the first study to use the UVP6 as a continuous recorder. Typically, this instrument is used for discrete particle measurements in the open ocean (Stemmann et al., 2012). To validate the data generated by this instrument, we compared them with other parameters that can indicate the presence of aggregates, such as the carbon transport toward the seafloor measured on sediment trap samples. Carbon fluxes are not exclusively related to the formation and sedimentation of aggregates, but can also be associated with free phytoplankton cells or detrital material (Durkin et al., 2016). Nonetheless, several major POC transport events took place at the same time as detected aggregation events (Fig. 5). On the other hand, the POC transport that took place in late May might have been caused, by the collapse of *Guinardia* spp. or cells of other species present in lower amounts (Fig. 6B). This corroborates the interpretation of the data on aggregate concentration produced by the UVP.

At Lanvéoc in 2021, eight major periods were detected during which significant amounts of aggregates were present in the water column. Each of these episodes occurred a few days after the formation of a diatom bloom. For example, the first event occurred on 30 March following a *Co. wailesii* bloom that occurred on mid/late March, and the third aggregation event occurred in late April, a few days after a *C. pelagica* bloom (Fig. 6B). These results are consistent with the observation that aggregates could be formed at the end of phytoplankton blooms, which is also in line with the validation based on UVP6 data.

As explained above, the formation of aggregates can occur at the end of phytoplankton blooms, i.e., when the cells decayed under highly stressful conditions (e.g. Alldredge et al., 1993; Passow and Alldredge, 1994; Passow, 2002). Several factors can explain the formation of these aggregates in the water column at Lanvéoc in 2021, including nutrient limitation and allelopathic interactions.

It can be observed that nutrient limitation preceded most aggregation events. For instance, the first aggregation episode in late March occurred when phosphate became the limiting factor in the water column. Similarly, the second and third aggregation episodes occurred when DIN and  $\text{Si}(\text{OH})_4$  became limiting in early and mid-April, respectively (Fig. 3A). Finally, the main diatom bloom detected in early June (Fig. 6B) was likely initiated by a re-enrichment in  $\text{Si}(\text{OH})_4$ . Then, this nutrient became limiting again, leading to the collapse of the bloom, triggering the formation of the subsequent aggregates. However, nutrient stress is not the only parameter that can induce a stress and explain the formation of aggregates in the water column.

When several phytoplankton species develop at the same time, some of them can have a negative effect on the development of others, becoming a source of stress contributing to their collapse and the subsequent formation of aggregates (Legrand et al., 2003). Some species of mixotrophic or heterotrophic dinoflagellates are known to have so-called allelopathic effects, specifically species in the genus *Gymnodinium* (*G. impudicum*, Band-Schmidt et al., 2020; *G. nagasakiense* (now named *Karenia mikimotoi*), Legrand et al., 2003). In the present study, the most frequently encountered dinoflagellates belonged to *Gymnodinium* (55% of total dinoflagellate), a common genus found in the Bay of Brest (e.g., Chauvaud et al., 1998; Fröhlich et al., 2022a) (Fig. 6C). Although aggregation episodes occurring on 30 March and 27 April could have been caused by nutrient limitation stress, the simultaneous

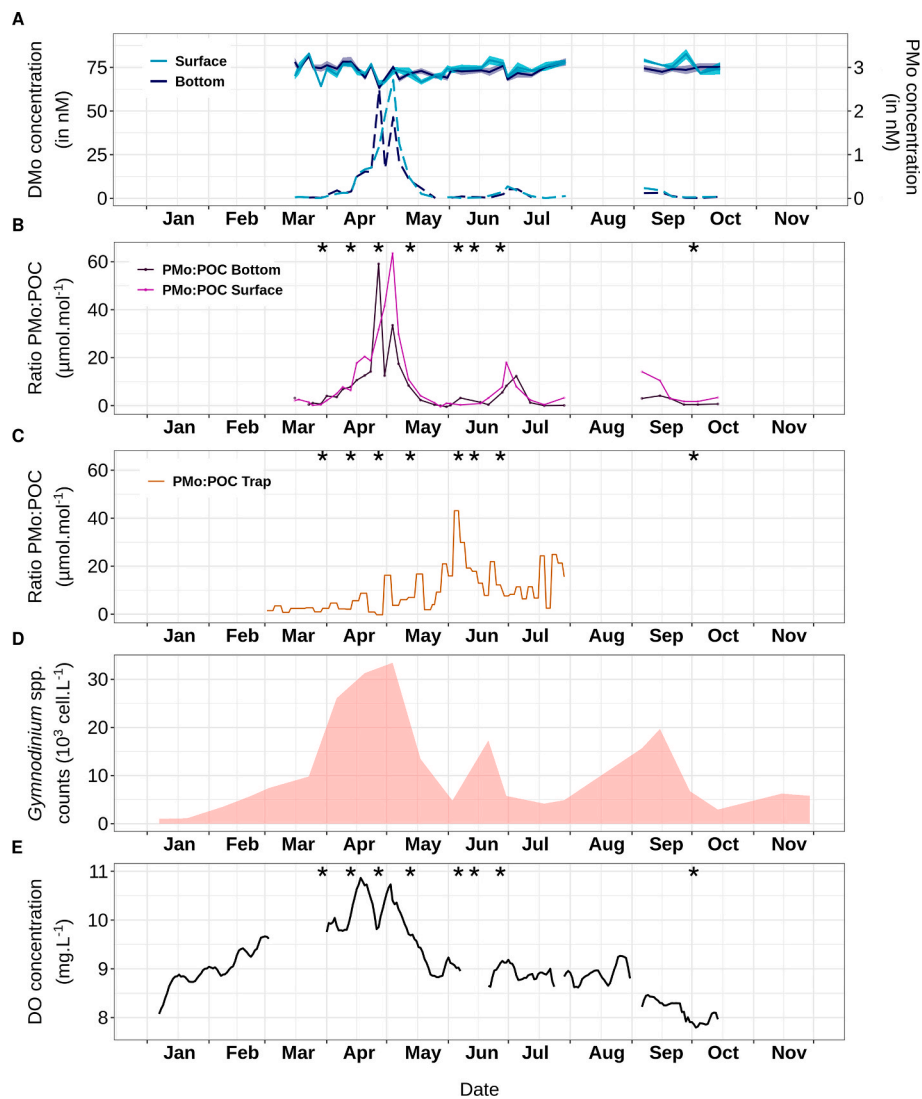


**Fig. 8.** Temporal variations of (A) normalized dissolved molybdenum (DMonorm) and particulate molybdenum (PMo) concentrations, (B) particulate molybdenum-to-POC (PMo:POC) ratios measured in the water column and (C) in the sediment trap samples, (D) *Gymnodinium* spp. cell concentration, and (E) dissolved oxygen (DO) concentration. Black asterisks represent the eight aggregation events that were defined in Section 3.3. (two columns).

development of *Gymnodinium* may also have favoured cell agglomeration (Fig. 6C). This phenomenon can also be observed for the aggregates that formed on 26 June, when a significant development of *Gymnodinium* spp. took place at the same time as the bloom of the diatom *Chaetoceros* spp. (Fig. 4B and C).

Finally, other parameters that were not quantified in this study, such as hydrodynamics, light stress, viruses, intense grazing activities by zooplankton and the production of fecal pellets, or higher microbial activity could also initiate the formation of aggregates (e.g., Passow, 2002; Lunau et al., 2006; Arsenieff et al., 2022). It is thus important to study variation in phytoplankton assemblages as well as the chemical or physical conditions of the water column to better understand what triggers aggregation.

#### 4.2. Relationship of molybdenum dynamics with primary producers

Mo concentrations in the dissolved ( $DMo_{norm}$  range: 60–80 nM) and particulate (PMo:POC range: 0–60  $\mu\text{mol mol}^{-1}$ ) fractions measured at Lanvéoc in 2021 (Fig. 8A and B) were comparable to data collected in 2011 (Waeles et al., 2013; Thébaud et al., 2022). The DMo concentration is below values expected for a conservative mixing at salinity 32–35 as measured in situ during our survey (Siebert et al., 2023), resulting in a

DMo deficit of about 20–40% as observed at the same site in 2011 (Waeles et al., 2013). Various explanations have been proposed for this deficit, including biological processes such as phytoplankton assimilation, as well as physico-chemical processes such as scavenging on phytoplankton aggregates. In parallel, several episodes of PMo:POC enrichment as well as one major episode of high PMo transport were detected in surface and bottom waters (Fig. 8B and C). The reasons behind these signals are discussed below.

##### 4.2.1. Impact of phytoplankton cells on molybdenum concentrations

Given that the phytoplankton community structure changed on short time-scales, the chemistry of the water column is expected to be strongly affected by the succession of microalgal species. Here, we aimed to identify one or several species that would explain the three PMo:POC peaks (Fig. 8B). The best candidate was the dinoflagellate *Gymnodinium*, which bloomed thrice in 2021 (in late April, in mid/late June and in early/mid September) (Fig. 8D). PMo:POC peaks were recorded in late April, late June and early September, i.e., the dates between *Gymnodinium* blooms and PMo:POC peaks almost match exactly (Fig. 8B and D). The reason for this slight mismatch may be that the frequency of phytoplankton identification and counts was too low (one measurement every two weeks) to accurately capture the exact timing of the bloom.

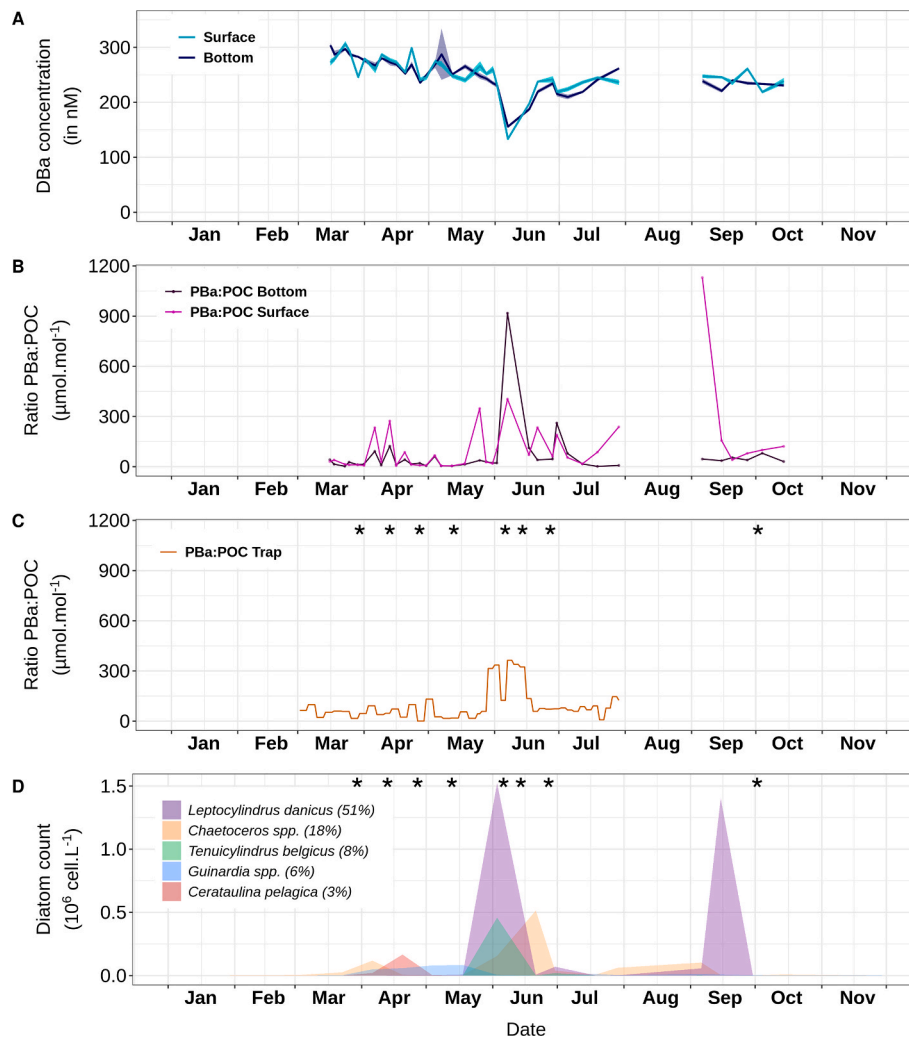


**Fig. 9.** Temporal variations of (A) dissolved barium (DBa) concentration, (B) particulate barium-to-POC ratios (PBa:POC) measured in the water column and (C) in the sediment trap samples, and (D) concentrations of the main diatom species (with their relative abundance among the bulk of diatoms). Black asterisks represent the eight aggregation events that were defined in Section 3.3. (two columns).

Previous studies have suggested that *Gymnodinium* cells could impact Mo dynamics of the water column. For instance, Fröhlich et al. (2022a) proposed that the Mo peaks measured in *Pecten maximus* shells are linked to the presence of *Gymnodinium* spp. cells and different reasons can explain this link. Firstly, the cells from this genus have been reported to be naturally enriched in Mo in comparison to other phytoplankton taxa (Ho et al., 2003). For example, in this latter study, *Gymnodinium chlorophorum* (renamed *Lepidodinium chlorophorum*) showed an Mo content 2.7 times higher than *Thalassiosira eccentrica*, the second most Mo-rich phytoplankton species reported by the authors. Overall, microalgae cells have a greater affinity with ammonia because it is the form of nitrogen that requires the least energy to assimilate even if phytoplankton cells can assimilate nitrate. Nonetheless, *Gymnodinium* cells present a higher affinity with nitrate (Yamamoto et al., 2004), which is the nitrogen source that supports fastest growth for this genus; in contrast, ammonium leads to a growth rate that is two times lower (Yamaguchi and Itakura, 1999). The assimilation of nitrate requires the synthesis of an enzyme, nitrate reductase, of which Mo is an essential co-factor (e.g. Nicholas and Nason, 1955; Eppley et al., 1969). At Lanvéoc in 2021, the first two *Gymnodinium* blooms occurred simultaneously with a slight decrease of DMo<sub>norm</sub> concentrations in the water column and an increase in PMo:POC values, suggesting a higher Mo uptake due to the presence of a higher amount of cells (Fig. 8A and B and D). Furthermore, the high affinity of *Gymnodinium* cells with nitrate was

also visible because this first two blooms collapsed when nitrate concentrations fell below 0.1 μmol L<sup>-1</sup> (0.06 μmol L<sup>-1</sup> in late April and 0.09 μmol L<sup>-1</sup> in late June; Fig. 3B), which is the concentration below which nitrate uptake is likely impossible for most phytoplankton species (Rhee, 1974). This relationship may contribute to explain why DMo<sub>norm</sub> concentrations decreased during the first two *Gymnodinium* blooms, simultaneously to the increase in PMo:POC (Fig. 8B), suggesting a Mo uptake for the synthesis of nitrate reductase.

#### 4.2.2. Aggregate involvement in molybdenum sedimentation

Mo is among the best studied redox-sensitive element. Although its behaviour in coastal waters has already been documented, processes controlling its dynamics are still poorly understood (e.g., Adelson et al., 2001; Dellwig et al., 2007; Kowalski et al., 2013; Waeles et al., 2013). Scavenging on Mn oxides has long been advanced as a possible explanation for this DMo deficit in reducing waters (Berrang and Grill, 1974). However in coastal sites of the Wadden Sea, Dellwig et al. (2007) did not find strong evidence of a relation between Mn-oxidation and Mo depletion. At Lanvéoc, Waeles et al. (2013) attributed a similar removal of DMo, to Mo adsorption on iron oxides, a process occurring in the inner Aulne estuary. Moreover, the PMo concentrations, in the range of 0–0.5 nM throughout the year, as well as the maximum PMo peak measured during the survey in late April (up to 2.5 nM; Fig. 8A) were too low to completely explain such a DMo deficit and to influence DMo

concentration.

Mo mainly occurs as stable molybdate ion ( $\text{MoO}_4^{2-}$ ) in well-oxygenated waters. On the other hand, it could be found enriched in anoxic and euxinic sediments (Helz et al., 1996; Morford and Emerson, 1999; Chaillou et al., 2002). In euxinic conditions, thiolation of Mo is thought to be the reason of its higher reactivity towards particles allowing its important scavenging (Adelson et al., 2001; Tribouillard et al., 2004). Previous studies have shown that marine aggregates could be significantly depleted in oxygen in comparison to the surrounding waters (Allredge and Cohen, 1987; Ploug et al., 1997; Ploug, 2001). They can also reach euxinic conditions as found by Shanks and Reeder (1993) with significant sulphide concentrations of about 25  $\mu\text{M}$ . The onset of euxinic conditions within aggregates should be determinant to promote the conversion of Mo, by thiolation, from DMo species (in the water inside the aggregates) towards PMo species (in the matrix of the aggregates).

In the present study, the aggregate dynamics was assessed using the UVP6 (Fig. 7). Three of the eight aggregation episodes led to a significant transport of PMo toward the seafloor (Fig. 8C). Although the different aggregation episodes were observed in well-oxygenated waters, some of them were associated with the occurrence of very large aggregates (Fig. 7). Indeed, those formed in June would be more oxygen-depleted in comparison to late April aggregates. Combined with the potential production of sulphide within these particles, these aggregates would scavenge higher amounts of Mo, resulting in the observed Mo transport (Fig. 8C). Nonetheless, it is noteworthy that the oxygen measurements were performed in the vicinity of the sediment, and this may not reflect the actual concentrations of the water column. Moreover, oxygen as well as sulphide concentration within aggregates formed during our survey were not quantified, preventing us from providing more relevant hypothesis.

Adelson et al. (2001) proposed some hypotheses that could explain the scavenging and fixation of  $\text{MoO}_4^{2-}$  in the anoxic Chesapeake Bay sediments.  $\text{MoO}_4^{2-}$  ions could diffuse from the water column until they encounter organic thiols or  $\text{H}_2\text{S}$  at sufficient concentration. As a result,  $\text{MoO}_4^{2-}$  would be converted to a solid form including thiomolybdates and/or inorganic Mo–Fe–S clusters (Adelson et al., 2001). Within the aggregates of the Bay of Brest, it is more probable that the excess Mo is associated with thiols because the formation of inorganic Mo–Fe–S clusters is thought to require the occurrence of  $\text{FeS}_2$  at significant levels (Adelson et al., 2001), which seems very unlikely here. These organic thiols could be found on the organic matrix of these aggregates (i.e., EPS). Therefore, the production of EPS, which are known to present high affinities with trace elements or metals (Decho, 1990), could cause Mo enrichment in aggregates, and therefore an increase of the PMo content in the water column. But while large aggregates may be ideal micro-environments for such scavenging of DMo, they are not sampled using Niskin bottles and may be undersampled in sediment traps with a 154  $\text{cm}^2$  opening as the one used in the current study (Drago, 2023), explaining why the observed DMo deficit may not be reflected by a similar increase of the PMo.

This latter assumption still needs to be addressed and the relationship between Mo and aggregates remains poorly understood in coastal ecosystems as well as the associated chemical processes. To better understand the underlying mechanism, the trace element content of differently sized aggregates and data on their exact oxygen and sulphide content are needed. However, in the natural environment, this type of study may be very challenging, because large aggregates are undersampled by common sediment traps and in situ sampling of single aggregates by divers is extremely difficult due to their fragility. However, laboratory studies using rolling tanks (e.g., Moriceau et al., 2007; De La Rocha et al., 2008) or mesocosms (Mori et al., 2021) can overcome these issues and investigate the chemical composition of individual aggregates. For example, experiments using monospecific and/or plurispecific phytoplankton strains (with or without zooplankton to quantify the impacts of fecal pellets production on aggregation processes) could

assess the interaction of Mo with aggregates as well as the associated chemical processes involved (i.e., precipitation, adsorption, scavenging etc.). These experiments would be very important to refine our knowledge on how aggregation influences the availability of Mo for organisms and its transport toward the seafloor.

#### 4.3. Relationship between barium and phytoplankton dynamics

In the Bay of Brest, Ba concentrations have never been measured or reported. However, the total Ba values measured at Lanvéoc during our study (on average, approx. 250 nM) are in agreement with the range commonly observed in other coastal ecosystems, i.e., approx. 100–200 nM as recorded in the Humber, Chesapeake or Delaware estuaries (Coffey et al., 1997). At Lanvéoc, successive periods of enrichment in PBa:POC were detected in bottom and surface waters including a major event that took place in early June, when a sudden increase in PBa:POC and drop in DBa were detected (Fig. 9A and B). According to Waeles et al. (2013), particulate Pb (PPb) can be considered as a good proxy of lithogenic suspended particulate matter in the Aulne estuary. This element has been measured following the same method as PMo and PBa measurements (Waeles, M., unpublished). Comparison of PBa values to PPb values showed that this early June bloom was associated with high PBa:PPb ratio (up to 27) which was well above the lithogenic background ratio of 2.

Ba is not known to be an essential element for the proper functioning of phytoplankton cells (Sternberg et al., 2005). Nonetheless, several studies have recorded an accumulation of Ba in various species, generally attributed to the adsorption of  $\text{Ba}^{2+}$  onto the silica matrix of diatoms (Dehairs et al., 1980; Fisher et al., 1991; Ganeshram et al., 2003; Sternberg et al., 2005). Adsorption can also occur on ferric hydroxides (as long as the environmental parameters allow their precipitation), which are associated with the surface of the diatom cells (Sternberg et al., 2005). DBa would then move into the particulate fraction when diatom frustules form and return into the dissolved phase during dissolution of frustules after cell decay. However, some Ba would remain in the particulate fraction because frustule dissolution is a process that requires more time than POC degradation (Moriceau et al., 2009; Bourtou et al., 2016), or because barite crystals are formed (Dehairs et al., 1980). In the present study, the main PBa:POC peak recorded in early June (Fig. 9B) corresponded to the timing of the main diatom bloom (Fig. 9D), alongside a peak in PBa:POC in surface and bottom waters (Fig. 9B). Therefore, Ba was likely bound to *L. danicus*, *T. belgicus* or *Chaetoceros* spp. cells, which are the dominant species found in early June (Fig. 9D). A few days later, the bloom collapsed and the cells decayed, which was accompanied by a low Chl:Pheo ratio and a high Chl:POC value on mid-June (Fig. 4). These values indicated a high phytoplankton degradation rate and a reduction in the effectiveness of photosynthesis, respectively, especially in bottom waters after the bloom. A portion of the diatom-linked Ba would then have returned to the dissolved fraction, with approx. 2–4% forming barite crystals (Ganeshram et al., 2003). These dynamics are also revealed by the DBa data of surface and bottom waters (Fig. 9A). Before the depletion (260 nM in surface and 231 nM in bottom water), concentrations were 7% and 5% higher than after depletion, in surface (242 nM) and bottom (220 nM) water, respectively. Some of the Ba released by the phytoplankton may thus remain in the particulate fraction and form barite crystals. Even if the Ba that precipitated as barite crystals remained at a higher proportion than that recorded by Ganeshram et al. (2003), the values from our study represent approximations, because the method used here is not appropriate to accurately capture the amount of Ba that precipitates as barite crystals. Another explanation could be that even if a significant amount of the diatom-linked Ba would have returned to the dissolved fraction after the collapse of the early June bloom, a portion of Ba might remain trapped on diatom frustules since they are not all instantaneously dissolved on such short time scales. Furthermore, the fact that samples before and after these events were recovered under

different tidal states might also explain this offset. In addition to this main event, other PBa:POC elevations may be related to diatom blooms. In particular, the PBa:POC peaks that occurred on early and mid-April were synchronous to the first elevation in the diatoms counts (mainly composed with *Chaetoceros* spp. and *C. pelagica*; Fig. 9D), and that the mid/late June PBa:POC peaks in surface water was synchronous with the *Chaetoceros* spp. bloom (Fig. 9D). At these time intervals, the adsorption process may be similar to the mechanism described above, but lower in scale, because the recorded blooms were not as intense as the early June diatom bloom and also because diatom species may have different abilities of trapping Ba (due to differences in frustule surface area, composition or thickness). However, some other PBa:POC peaks (e.g., late May, late June) were not strictly aligned with a diatom bloom and potential reasons for this will be discussed further below (Fig. 8B and D).

Because the presence of diatoms in the water column has an impact on the temporal variation of Ba in the ecosystem, diatoms are likely involved in the transport of that element to the SWI. Based on the Pba:POC<sub>trap</sub> data (Fig. 9C), it appears that a major Ba transport event took place simultaneously with the early June diatom bloom. To verify this hypothesis, the Bsi:POC<sub>trap</sub> ratio was used to assess if the main Ba transport was induced by diatoms. The typical Si:C value of a mono-specific culture of *L. danicus* is 0.11 (Brzezinski, 1985), which roughly corresponds to the Bsi:POC<sub>trap</sub> value measured at the same time (0.08 on 1–3 June; 0.10 on 4–6 June; 0.12 on 7–9 June; Fig. 5). This pattern suggests that the main episode of Ba transport was linked to the early June diatom bloom which is mainly composed with *L. danicus* (68%) alongside other less abundant species such as *Chaetoceros* spp. (7%), which present similar Si:C ratios (Brzezinski, 1985), or *T. belgicus* (21%) (Fig. 9D). These results are also in line with the fact that not all diatoms adsorb Ba in the same way; Ba content of cells varies among species (Fisher et al., 1991). However, interpretations of Bsi:POC results recorded in natural environment to track diatom cells must be approached with caution, as other parameters can also influence variations of this ratio (e.g., sponge spicules).

Other parameters can explain some of the PBa:POC peaks observed and the differences in PBa:POC signals between bottom and surface waters (Fig. 9B). Specifically, the PBa:POC peak measured in early June was twice as high in bottom water as in surface water and our data cannot be used to explain the underlying reason. Nevertheless, other phytoplankton species, possibly not detected with the current sampling method, may be present at the onset of the Ba enrichment in the water column. For example, coccolithophorids are phytoplankton organisms with an external calcium carbonate skeleton (see Paasche (2001) for review), that is known to partition Ba (Langer et al., 2009). We did not detect coccolithophorids in this study, but this does not necessarily mean that they were absent since coccolithophorids cells have already been observed in the past in the Bay of Brest. Cell counts were only measured in the surface layer, but due to the high density of the cell skeleton, their sedimentation rate is much higher than that of other phytoplankton taxa (Young, 1994). Coccolithophorids are therefore common in bottom waters, which may explain why the Ba peak in early June was twice as high near the seafloor than in surface water. In addition, the use of acidic Lugol's rather than neutral Lugol's, may have partially degraded the coccoliths prior to analysis, rendering them unidentifiable under the microscope. Finally, other organisms such as zooplankton may also have the ability to adsorb Ba onto their exoskeletons and cause the formation of barite crystals after death, e.g., acantharians (Bernstein and Byrne, 2004). Nonetheless, their presence and dynamics have never been officially reported or studied in the Bay of Brest. Finally, even if typical phytoplankton dynamics were recorded at Lanvéoc in 2021, it would be interesting to renew that type of environmental survey to confirm or not the hypotheses put forward so far, because phytoplankton community structures can vary from one year to another, with differences in the main diatom species at Lanvéoc being either *Chaetoceros* spp. or *L. danicus* (Thébault et al., 2022; Fröhlich

et al., 2022a).

## 5. Conclusion and perspectives

The present study reported Mo and Ba concentrations in the water column in the Bay of Brest between mid-March and mid-October 2021. Our results suggest that phytoplankton dynamics significantly influence the availability of particulate Mo and Ba for primary consumers and benthic organisms. We corroborated the hypothesis that Mo is linked to aggregation episodes, although our results suggest that not all aggregates transport significant amounts of Mo toward the SWI. Apparently, large and therefore more oxygen-depleted aggregates associated with the presence of sulphide compounds would be at the origin of Mo scavenging and the transport of this element to the seafloor. Moreover, *Gymnodinium* spp. are present at the onset of the changes in Pmo:POC content in the water column. On the other side, the enrichment of Pba and depletion of DBa was most likely associated with diatom cells. Furthermore, aggregation episodes may also be vectors facilitating the transport of Ba to the sediment. Understanding the processes behind the enrichment of Mo and Ba in the water column requires future monitoring surveys, allowing comparisons between years and thus the detection of common patterns. Furthermore, aggregates should be artificially generated in the laboratory using rolling tanks to test the hypotheses raised by our results. These new findings might be very helpful for interpreting temporal variations of Mo and Ba measured in the shells of *Pecten maximus* specimens to reconstruction past phytoplankton dynamics in the Bay of Brest, which is the subject of recent investigations (Fröhlich et al., 2022a, 2022b; Thébault et al., 2022).

## CRediT authorship contribution statement

**Valentin Siebert:** Writing – review & editing, Writing – original draft, Investigation, Formal analysis, Data curation, Conceptualization. **Lukas Fröhlich:** Writing – review & editing, Investigation, Conceptualization. **Julien Thébault:** Writing – review & editing, Supervision, Project administration, Funding acquisition, Conceptualization. **Bernard R. Schöne:** Writing – review & editing, Supervision, Project administration, Conceptualization. **Gaspard Delebecq:** Writing – review & editing, Formal analysis, Data curation. **Marc Picheral:** Writing – review & editing, Methodology, Data curation. **Matthieu Waeles:** Writing – review & editing, Methodology, Data curation. **Brivaëla Moriceau:** Writing – review & editing, Supervision, Conceptualization.

## Declaration of competing interest

The authors declare that they have no known competing financial interests or personal relationships that could have appeared to influence the work reported in this paper.

## Data availability

Data available in the SEANOE (SEA scieNtific Open data Edition) repository: <https://www.seanoe.org/data/00808/92043/> (Siebert et al., 2023)

## Acknowledgements

We kindly acknowledge Manon Le Goff, Émilie Grossteffan, Isabelle Bihannic, Kévin Bihannic, Jérémy Devesa and Morgane Gallinari from the PACHIDERM platform (Plateau d'Analyse CHimique de l'EnviRonnement Marin) for seawater analyses. We are also very grateful to Marie-Laure Rouget and Yoan Germain (Pôle Spectrométrie Océan) for their help in the analyses of trace element concentrations in seawater samples. We also thank the SCUBA divers Erwan Amice and Thierry Le Bec as well as the R/V *Albert Lucas* crew, without whom it would have been impossible to collect the samples and carry out the environmental

monitoring. We are deeply grateful to Tim Jennerjahn (Editor) and Dianne Greenfield (Associate Editor) for demonstrating so much patience and understanding throughout the review process. We also extend our gratitude to two anonymous reviewers for their thorough critiques and immensely valuable comments, which significantly enhanced the manuscript.

This work was funded by the French National Research Agency (ANR - ANR-18-CE92-0036-01) and the German Research Foundation (DFG - SCHO793/21) with the support of the Bretagne Regional Council. This study was carried out as part of the collaborative French-German project HIPPO (HIGH-resolution Primary Production multiprOxy archives). A CC-BY public copyright license has been applied by the authors to the present document and will be applied to all subsequent versions up to the Author Accepted Manuscript arising from this submission, in accordance with the grant's open access conditions.

## References

- Adelson, J.M., Helz, G.R., Miller, C.V., 2001. Reconstructing the rise of recent coastal anoxia; molybdenum in Chesapeake Bay sediments. *Geochem. Cosmochim. Acta* 65, 237–252. [https://doi.org/10.1016/S0016-7037\(00\)00539-1](https://doi.org/10.1016/S0016-7037(00)00539-1).
- Allredge, A.L., Cole, J.J., Caron, D.A., 1986. Production of heterotrophic bacteria inhabiting macroscopic organic aggregates (marine snow) from surface waters. *Limnol. Oceanogr.* 31, 68–78. <https://doi.org/10.4319/lo.1986.31.1.0068>.
- Allredge, A.L., Cohen, Y., 1987. Can microscale chemical patches persist in the sea? Microelectrode study of marine snow, fecal pellets. *Science* 235, 689–691. <https://doi.org/10.1126/science.235.4789.689>.
- Allredge, A.L., Silver, M.W., 1988. Characteristics, dynamics and significance of marine snow. *Prog. Oceanogr.* 20, 41–82. [https://doi.org/10.1016/0079-6611\(88\)90053-5](https://doi.org/10.1016/0079-6611(88)90053-5).
- Allredge, A.L., Gotschalk, C., 1990. The relative contribution of marine snow of different origins to biological processes in coastal waters. *Continent. Shelf Res.* 10, 41–58. [https://doi.org/10.1016/0278-4343\(90\)90034-J](https://doi.org/10.1016/0278-4343(90)90034-J).
- Allredge, A.L., Passow, U., Logan, B.E., 1993. The abundance and significance of a class of large, transparent organic particles in the ocean. *Deep-Sea Res. Part I* 40, 1131–1140. [https://doi.org/10.1016/0967-0637\(93\)90129-Q](https://doi.org/10.1016/0967-0637(93)90129-Q).
- Arsenieff, L., Kimura, K., Kranzler, C.F., Baudoux, A.-C., Thamatrakoln, K., 2022. Diatom viruses. In: Falcitore, A., Mock, T. (Eds.), *The Molecular Life of Diatoms*. Springer, Cham, pp. 713–740.
- Band-Schmidt, C.J., Zumaya-Higuera, M.G., López-Cortés, D.J., Leyva-Valencia, I., Quijano-Scheggia, S.I., Hernández-Guerrero, C.J., 2020. Allelopathic effects of *Margalefidinium polykrikoides* and *Gymnodinium impudicum* in the growth of *Gymnodinium catenatum*. *Harmful Algae* 96, 101846. <https://doi.org/10.1016/j.hal.2020.101846>.
- Barats, A., Amouroux, D., Chauvaud, L., Pêcheyran, C., Lorrain, A., Thébault, J., Church, T.M., Donard, O.F.X., 2009. High frequency Barium profiles in shells of the Great Scallop *Pecten maximus*: a methodical long-term and multi-site survey in Western Europe. *Biogeosciences* 6, 157–170. <https://doi.org/10.5194/bg-6-157-2009>.
- Bentaleb, I., Fontugne, M., Descolas-Gros, C., Girardin, C., Mariotti, A., Pierre, C., Brunet, C., Poisson, A., 1998. Carbon isotopic fractionation by plankton in the Southern Indian Ocean: relationship between  $\delta^{13}\text{C}$  of particulate organic carbon and dissolved carbon dioxide. *J. Mar. Syst.* 17, 39–58. [https://doi.org/10.1016/S0924-7963\(98\)00028-1](https://doi.org/10.1016/S0924-7963(98)00028-1).
- Bernstein, R.E., Byrne, R.H., 2004. Acantharians and marine barite. *Mar. Chem.* 86, 45–50. <https://doi.org/10.1016/j.marchem.2003.12.003>.
- Berrang, P.G., Grill, E.V., 1974. The effect of manganese oxide scavenging on molybdenum in Saanich Inlet, British Columbia. *Mar. Chem.* 2, 125–148. [https://doi.org/10.1016/0304-4203\(74\)90033-4](https://doi.org/10.1016/0304-4203(74)90033-4).
- Boutorh, J., Moriceau, B., Gallinari, M., Ragueneau, O., Bucciarelli, E., 2016. Effect of trace metal-limited growth on the postmortem dissolution of the marine diatom *Pseudo-nitzschia delicatissima*. *Global Biogeochem. Cycles* 30, 57–69. <https://doi.org/10.1002/2015GB005088>.
- Boyce, D.G., Lewis, M.R., Worm, B., 2010. Global phytoplankton decline over the past century. *Nature* 466, 591–596. <https://doi.org/10.1038/nature09268>.
- Brzezinski, M.A., 1985. The Si:C:N ratio of marine diatoms: interspecific variability and the effect of some environmental variables. *J. Phycol.* 21, 347–357. <https://doi.org/10.1111/j.0022-3646.1985.00347.x>.
- Carlson, C.A., Ducklow, H.W., Michaels, A.F., 1994. Annual flux of dissolved organic carbon from the euphotic zone in the northwestern Sargasso Sea. *Nature* 371, 405–408. <https://doi.org/10.1038/371405a0>.
- Chaillou, G., Anschutz, P., Lavaux, G., Schäfer, J., Blanc, G., 2002. The distribution of Mo, U, and Cd in relation to major redox species in muddy sediments of the Bay of Biscay. *Mar. Chem.* 80, 41–59. [https://doi.org/10.1016/S0304-4203\(02\)00097-X](https://doi.org/10.1016/S0304-4203(02)00097-X).
- Charpy-Roubaud, C., Sournia, A., 1990. The comparative estimation of phytoplanktonic, microphytobenthic and macrophytobenthic primary production in the oceans. *Mar. Microb. Food Webs* 4, 31–57.
- Chauvaud, L., Thouzeau, G., Pautet, Y.-M., 1998. Effects of environmental factors on the daily growth rate of *Pecten maximus* juveniles in the Bay of Brest (France). *J. Exp. Mar. Biol. Ecol.* 227, 83–111. [https://doi.org/10.1016/S0022-0981\(97\)00263-3](https://doi.org/10.1016/S0022-0981(97)00263-3).
- Coffey, M., Dehairs, F., Collette, O., Luther, G., Church, T., Jickells, T., 1997. The behaviour of dissolved barium in estuaries. *Estuar. Coast Shelf Sci.* 45, 113–121. <https://doi.org/10.1006/ecss.1996.0157>.
- Dam, H.G., Drapeau, D.T., 1995. Coagulation efficiency, organic-matter glues and the dynamics of particles during a phytoplankton bloom in a mesocosm study. *Deep-Sea Res. Part II* 42, 111–123. [https://doi.org/10.1016/0967-0645\(95\)00007-D](https://doi.org/10.1016/0967-0645(95)00007-D).
- De La Rocha, C.L., Nowald, N., Passow, U., 2008. Interactions between diatom aggregates, minerals, particulate organic carbon, and dissolved organic matter: further implications for the ballast hypothesis. *Global Biogeochem. Cycles* 22, GB4005. <https://doi.org/10.1029/2007GB003156>.
- Decho, A.W., 1990. Microbial exopolymer secretions in ocean environments: their role(s) in food webs and marine processes. *Oceanogr. Mar. Biol. Annu. Rev.* 28, 73–153.
- Dehairs, F., Chesselet, R., Jedwab, J., 1980. Discrete suspended particles of barite and the barium cycle in the open ocean. *Earth Planet Sci. Lett.* 49, 528–550. [https://doi.org/10.1016/0012-821X\(80\)90094-1](https://doi.org/10.1016/0012-821X(80)90094-1).
- Del Amo, Y., Le Pape, O., Tréguier, P., Quéguiner, B., Ménesguen, A., Aminot, A., 1997. Impacts of high-nitrate freshwater inputs on macrotidal ecosystems. I. Seasonal evolution of nutrient limitation for the diatom-dominated phytoplankton of the Bay of Brest (France). *Mar. Ecol. Prog. Ser.* 161, 213–224. <https://doi.org/10.3354/meps161213>.
- Dellwig, O., Beck, M., Lemke, A., Lunau, M., Kolditz, K., Schnetger, B., Brumsack, H.J., 2007. Non-conservative behaviour of molybdenum in coastal waters: coupling geochemical, biological, and sedimentological processes. *Geochem. Cosmochim. Acta* 71, 2745–2761. <https://doi.org/10.1016/j.gca.2007.03.014>.
- Diercks, A.R., Asper, V.L., 1997. In situ settling speeds of marine snow aggregates below the mixed layer: black Sea and Gulf of Mexico. *Deep-Sea Res. Part I* 44, 385–398. [https://doi.org/10.1016/S0967-0637\(96\)00104-5](https://doi.org/10.1016/S0967-0637(96)00104-5).
- Doré, J., Thébault, J., Roy, V., Dewilde, F., Chaillou, G., 2021. Insight into shell growth dynamics of *Macromeris polymya* in the St. Lawrence Estuary using sclerochemistry. *Mar. Chem.* 234, 103987. <https://doi.org/10.1016/j.marchem.2021.103987>.
- Drago, L., 2023. Analyse globale de la pompe à carbone biologique à partir de données en imagerie quantitative. Sorbonne Université, France. PhD Thesis.
- Durkin, C.A., Van Mooy, B.A.S., Dyhrman, S.T., Buesseler, K.O., 2016. Sinking phytoplankton associated with carbon flux in the Atlantic Ocean. *Limnol. Oceanogr.* 61, 1172–1187. <https://doi.org/10.1002/lno.10253>.
- Eppley, R.W., Coatsworth, J.L., Solórzano, L., 1969. Studies of nitrate reductase in marine phytoplankton. *Limnol. Oceanogr.* 14, 194–205. <https://doi.org/10.4319/lo.1969.14.2.0194>.
- Field, C.B., Behrenfeld, M.J., Randerson, J.T., Falkowski, P.G., 1998. Primary production of the biosphere: integrating terrestrial and oceanic components. *Science* 281, 237–240. <https://doi.org/10.1126/science.281.5374.237>.
- Fisher, N.S., Guillard, R.R.L., Bankston, D.C., 1991. The accumulation of barium by marine phytoplankton grown in culture. *J. Mar. Res.* 49, 339–354. <https://doi.org/10.1357/002224091784995882>.
- Fröhlich, L., Siebert, V., Huang, Q., Thébault, J., Jochum, K.P., Schöne, B.R., 2022a. Deciphering the potential of Ba/Ca, Mo/Ca and Li/Ca profiles in the bivalve shell *Pecten maximus* as proxies for the reconstruction of phytoplankton dynamics. *Ecol. Indic.* 141, 109121. <https://doi.org/10.1016/j.ecolind.2022.109121>.
- Fröhlich, L., Siebert, V., Walliser, E.O., Thébault, J., Jochum, K.P., Chauvaud, L., Schöne, B.R., 2022b. Ba/Ca profiles in shells of *Pecten maximus* - a proxy for specific primary producers rather than bulk phytoplankton. *Chem. Geol.* 593, 120743. <https://doi.org/10.1016/j.chemgeo.2022.120743>.
- Ganeshram, R.S., François, R., Commeau, J., Brown-Leger, S.L., 2003. An experimental investigation of barite formation in seawater. *Geochem. Cosmochim. Acta* 67, 2599–2605. [https://doi.org/10.1016/S0016-7037\(03\)00164-9](https://doi.org/10.1016/S0016-7037(03)00164-9).
- Garvey, M., Moriceau, B., Passow, U., 2007. Applicability of the FDA assay to determine the viability of marine phytoplankton under different environmental conditions. *Mar. Ecol. Prog. Ser.* 352, 17–26. <https://doi.org/10.3354/meps07134>.
- Gutiérrez, T., Biller, D.V., Shimmield, T., Green, D.H., 2012. Metal binding properties of the EPS produced by *Halomonas* sp. TG39 and its potential in enhancing trace element bioavailability to eukaryotic phytoplankton. *Biometals* 25, 1185–1194. <https://doi.org/10.1007/s10534-012-9581-3>.
- Helz, G.R., Miller, C.V., Charnock, J.M., Mosselmans, J.F.W., Patrick, R.A.D., Garner, C. D., Vaughan, D.J., 1996. Mechanism of molybdenum removal from the sea and its concentration in black shales: EXAFS evidence. *Geochem. Cosmochim. Acta* 60, 3631–3642. [https://doi.org/10.1016/0016-7037\(96\)00195-0](https://doi.org/10.1016/0016-7037(96)00195-0).
- Ho, T.Y., Quigg, A., Finkel, Z.V., Milligan, A.J., Wyman, K., Falkowski, P.G., Morel, F.M. M., 2003. The elemental composition of some marine phytoplankton. *J. Phycol.* 39, 1145–1159. <https://doi.org/10.1111/j.0022-3646.2003.03-090.x>.
- Jennings, B.R., Parslow, K., 1988. Particle size measurement: the equivalent spherical diameter. *Proc. Roy. Soc. Lond.* 419, 137–149. <https://doi.org/10.1098/rspa.1988.0100>.
- Kjørboe, T., Jackson, G.A., 2001. Marine snow, organic solute plumes, and optimal chemosensory behavior of bacteria. *Limnol. Oceanogr.* 46, 1309–1318. <https://doi.org/10.4319/lo.2001.46.6.1309>.
- Kowalski, N., Dellwig, O., Beck, M., Gräwe, U., Neubert, N., Nägler, T.F., Badewien, T.H., Brumsack, H.J., van Beusekom, J.E.E., Böttcher, M.E., 2013. Pelagic molybdenum concentration anomalies and the impact of sediment resuspension on the molybdenum budget in two tidal systems of the North Sea. *Geochem. Cosmochim. Acta* 119, 198–211. <https://doi.org/10.1016/j.gca.2013.05.046>.
- Kühn, S.F., Raven, J.A., 2008. Photosynthetic oscillation in individual cells of the marine diatom *Coscinodiscus walesii* (Bacillariophyceae) revealed by microsensor measurements. *Photosynth. Res.* 95, 37–44. <https://doi.org/10.1007/s11120-007-9221-x>.

- Langer, G., Nehrke, G., Thoms, S., Stoll, H., 2009. Barium partitioning in coccoliths of *Emiliania huxleyi*. *Geochem. Cosmochim. Acta* 73, 2899–2906. <https://doi.org/10.1016/j.gca.2009.02.025>.
- Laurenceau-Cornec, E.C., Trull, T.W., Davies, D.M., Bray, S.G., Doran, J., Planchon, F., Carlotti, F., Jouandet, M.-P., Cavagna, A.-J., Waite, A.M., Blain, S., 2015. The relative importance of phytoplankton aggregates and zooplankton fecal pellets to carbon export: insights from free-drifting sediment trap deployments in naturally iron-fertilised waters near the Kerguelen Plateau. *Biogeosciences* 12, 1007–1027. <https://doi.org/10.5194/bg-12-1007-2015>.
- Laurenceau-Cornec, E.C., Le Moigne, F.A.C., Gallinari, M., Moriceau, B., Toullec, J., Iversen, M.H., Engel, A., De La Rocha, C.L., 2020. New guidelines for the application of Stokes' models to the sinking velocity of marine aggregates. *Limnol. Oceanogr.* 65, 1264–1285. <https://doi.org/10.1002/lno.11388>.
- Lee, C., Hedges, J.I., Wakeham, S.G., Zhu, N., 1992. Effectiveness of various treatments in retarding microbial activity in sediment trap material and their effects on the collection of swimmers. *Limnol. Oceanogr.* 37, 117–130. <https://doi.org/10.4319/lno.1992.37.1.0117>.
- Legrand, C., Rengefors, K., Fistarol, G.O., Graneli, E., 2003. Allelopathy in phytoplankton-biochemical, ecological and evolutionary aspects. *Phycologia* 42, 406–419. <https://doi.org/10.2216/i0031-8884-42-4-406.1>.
- Logan, B.E., Passow, U., Alldredge, A.L., Grossart, H.P., Simont, M., 1995. Rapid formation and sedimentation of large aggregates is predictable from coagulation rates (half-lives) of transparent exopolymer particles (TEP). *Deep-Sea Res. Part II* 42, 203–214. [https://doi.org/10.1016/0967-0645\(95\)00012-F](https://doi.org/10.1016/0967-0645(95)00012-F).
- Lunau, M., Lemke, A., Dellwig, O., Simon, M., 2006. Physical and biogeochemical controls of microaggregate dynamics in a tidally affected coastal ecosystem. *Limnol. Oceanogr.* 51, 847–859. <https://doi.org/10.4319/lno.2006.51.2.0847>.
- McDonnell, A.M.P., Boyd, P.W., Buesseler, K.O., 2015. Effects of sinking velocities and microbial respiration rates on the attenuation of particulate carbon fluxes through the mesopelagic zone. *Global Biogeochem. Cycles* 29, 175–193. <https://doi.org/10.1002/2014GB004935>.
- Morford, J.L., Emerson, S., 1999. The geochemistry of redox sensitive trace metals in sediments. *Geochem. Cosmochim. Acta* 63, 1735–1750. [https://doi.org/10.1016/S0016-7037\(99\)00126-X](https://doi.org/10.1016/S0016-7037(99)00126-X).
- Mori, C., Beck, M., Striebel, M., Merder, J., Schnetger, B., Dittmar, T., Pahnke, K., Brumsack, H.J., 2021. Biogeochemical cycling of molybdenum and thallium during a phytoplankton summer bloom: a mesocosm study. *Mar. Chem.* 229, 103910. <https://doi.org/10.1016/j.marchem.2020.103910>.
- Moriceau, B., Garvey, M., Ragueneau, O., Passow, U., 2007. Evidence for reduced biogenic silica dissolution rates in diatom aggregates. *Mar. Ecol. Prog. Ser.* 333, 129–142. <https://doi.org/10.3354/meps333129>.
- Moriceau, B., Goutx, M., Guigue, C., Lee, C., Armstrong, R., Duflos, M., Tamburini, C., Charrière, B., Ragueneau, O., 2009. Si-C interactions during degradation of the diatom *Skeletonema marinoi*. *Deep-Sea Res. Part II* 56, 1381–1395. <https://doi.org/10.1016/j.dsr2.2008.11.026>.
- Moriceau, B., Laruelle, G.G., Passow, U., Van Cappellen, P., Ragueneau, O., 2014. Biogenic silica dissolution in diatom aggregates: insights from reactive transport modelling. *Mar. Ecol. Prog. Ser.* 517, 35–49. <https://doi.org/10.3354/meps11028>.
- Morris, A.W., 1975. Dissolved molybdenum and vanadium in the northeast Atlantic Ocean. *Deep Sea Res. Oceanogr. Abstr.* 22, 49–54. [https://doi.org/10.1016/0011-7471\(75\)90018-2](https://doi.org/10.1016/0011-7471(75)90018-2).
- Mykledal, S.M., 1995. Release of extracellular products by phytoplankton with special emphasis on polysaccharides. *Sci. Total Environ.* 165, 155–164. [https://doi.org/10.1016/0048-9697\(95\)04549-G](https://doi.org/10.1016/0048-9697(95)04549-G).
- Nicholas, D.J.D., Nason, A., 1955. Role of molybdenum as a constituent of nitrate reductase from soybean leaves. *Plant Physiol.* 30, 135–138. <https://doi.org/10.1104/pp.30.2.135>.
- Paasche, E., 2001. A review of the coccolithophorid *Emiliania huxleyi* (Prymnesiophyceae), with particular reference to growth, coccolith formation, and calcification-photosynthesis interactions. *Phycologia* 40, 503–529. <https://doi.org/10.2216/i0031-8884-40-6-503.1>.
- Passow, U., Alldredge, A.L., 1994. Distribution, size and bacterial colonization of transparent exopolymer particles (TEP) in the ocean. *Mar. Ecol. Prog. Ser.* 113, 185–198.
- Passow, U., 2002. Production of transparent exopolymer particles (TEP) by phyto- and bacterioplankton. *Mar. Ecol. Prog. Ser.* 236, 1–12. <https://doi.org/10.3354/meps236001>.
- Picheral, M., Catalano, C., Brousseau, D., Claustre, H., Coppola, L., Leymarie, E., Coindat, J., Dias, F., Fevre, S., Guidi, L., Irissou, J.O., Legendre, L., Lombard, F., Mortier, L., Penkerch, C., Rogge, A., Schmechtig, C., Thibault, S., Tixier, T., Waite, A., Stemmann, L., 2021. The Underwater Vision Profiler 6: an imaging sensor of particle size spectra and plankton, for autonomous and cabled platforms. *Limnol. Oceanogr. Methods* 20, 115–129. <https://doi.org/10.1002/lom3.10475>.
- Ploug, H., Kühl, M., Buchholz-Cleven, B., Jørgensen, B.B., 1997. Anoxic aggregates—an ephemeral phenomenon in the pelagic environment? *Aquat. Microb. Ecol.* 13, 285–294. <https://doi.org/10.3354/ame013285>.
- Ploug, H., 2001. Small-scale oxygen fluxes and remineralization in sinking aggregates. *Limnol. Oceanogr.* 46, 1624–1631. <https://doi.org/10.4319/lno.2001.46.7.1624>.
- Ploug, H., Iversen, M.H., Fischer, G., 2008. Ballast, sinking velocity, and apparent diffusivity within marine snow and zooplankton fecal pellets: implications for substrate turnover by attached bacteria. *Limnol. Oceanogr.* 53, 1878–1886. <https://doi.org/10.4319/lno.2008.53.5.1878>.
- Redfield, A.C., 1958. The biological control of chemical factors in the environment. *Am. Sci.* 46, 205–221.
- Rhee, G.Y., 1974. Phosphate uptake under nitrate limitation by *Scenedesmus* sp. and its ecological implications. *J. Phycol.* 10, 470–475. <https://doi.org/10.1111/j.1529-8817.1974.tb02742.x>.
- Sarthou, G., Timmermans, K.R., Blain, S., Tréguer, P., 2005. Growth physiology and fate of diatoms in the ocean: a review. *J. Sea Res.* 53, 25–42. <https://doi.org/10.1016/j.seares.2004.01.007>.
- Savoie, N., 2001. Origine et transfert de matière organique particulaire dans les écosystèmes littoraux macrotidaux). Université de Bretagne Occidentale, France. PhD Thesis.
- Shanks, A.L., Reeder, M.L., 1993. Reducing microzones and sulfide production in marine snow. *Mar. Ecol. Prog. Ser.* 96, 43–47.
- Siebert, V., Moriceau, B., Fröhlich, L., Schöne, B.R., Amice, E., Beker, B., Bihannic, K., Bihannic, I., Delebecq, G., Devesa, J., Gallinari, M., Germain, Y., Grossteffan, E., Jochum, K.P., Le Bec, T., Le Goff, M., Leynaert, A., Liorzou, C., Marec, C., Picheral, M., Rimmelin-Maury, P., Rouget, M.-L., Waeles, M., Thébaud, J., 2023. HIPPO environmental monitoring: impact of phytoplankton dynamics on water column chemistry and the sclerochronology of the king scallop (*Pecten maximus*) as a biogenic archive for past primary production reconstructions. *Earth Syst. Sci. Data* 15, 3263–3281. <https://doi.org/10.5194/essd-15-3263-2023>.
- Stemmann, L., Picheral, M., Guidi, L., Lombard, F., Prejger, F., Claustre, H., Gorsky, G., 2012. Assessing the spatial and temporal distributions of zooplankton and marine particles using the Underwater Vision Profiler. In: Le Galliard, J.-F., Guarini, J.-M., Gaill, F. (Eds.), *Sensors for Ecology - towards Integrated Knowledge of Ecosystems*, pp. 119–137.
- Sternberg, E., Tang, D., Ho, T.Y., Jeandel, C., Morel, F.M.M., 2005. Barium uptake and adsorption in diatoms. *Geochem. Cosmochim. Acta* 69, 2745–2752. <https://doi.org/10.1016/j.gca.2004.11.026>.
- Tabouret, H., Pomerleau, S., Jolivet, A., Pécuyer, C., Riso, R., Thébaud, J., Chauvaud, L., Amouroux, D., 2012. Specific pathways for the incorporation of dissolved barium and molybdenum into the bivalve shell: an isotopic tracer approach in the juvenile Great Scallop (*Pecten maximus*). *Mar. Environ. Res.* 78, 15–25. <https://doi.org/10.1016/j.marenvres.2012.03.006>.
- Tercier-Waerber, M.-L., Stoll, S., Slaveykova, V.I., 2012. Trace metal behavior in surface waters: emphasis on dynamic speciation, sorption processes and bioavailability. *Arch. Sci.* 65, 119–142. <https://doi.org/10.5169/seals-738356>.
- Thébaud, J., Chauvaud, L., L'Helgouen, S., Clavier, J., Barats, A., Jacquet, S., Pécuyer, C., Amouroux, D., 2009. Barium and molybdenum records in bivalve shells: geochemical proxies for phytoplankton dynamics in coastal environments? *Limnol. Oceanogr.* 54, 1002–1014. <https://doi.org/10.4319/lno.2009.54.3.1002>.
- Thébaud, J., Jolivet, A., Waeles, M., Tabouret, H., Sabarot, S., Pécuyer, C., Leynaert, A., Jochum, K.P., Schöne, B.R., Fröhlich, L., Siebert, V., Amice, E., Chauvaud, L., 2022. Scallop shells as geochemical archives of phytoplankton-related ecological processes in a temperate coastal ecosystem. *Limnol. Oceanogr.* 67, 187–202. <https://doi.org/10.1002/lno.11985>.
- Toullec, J., Moriceau, B., Vincent, D., Guidi, L., Lafond, A., Babin, M., 2021. Processes controlling aggregate formation and distribution during the Arctic phytoplankton spring bloom in Baffin Bay. *Elementa: Sci. Anthropocene* 9, 00001. <https://doi.org/10.1525/elementa.2021.00001>.
- Tribouillard, N., Riboulleau, A., Lyons, T., Baudin, F., 2004. Enhanced trapping of molybdenum by sulfurized marine organic matter of marine origin in Mesozoic limestones and shales. *Chem. Geol.* 213, 385–401. <https://doi.org/10.1016/j.chemgeo.2004.08.011>.
- Turner, J.T., 2015. Zooplankton fecal pellets, marine snow, phytodetritus and the ocean's biological pump. *Prog. Oceanogr.* 130, 205–248. <https://doi.org/10.1016/j.pocean.2014.08.005>.
- Vander Putten, E., Dehairs, F., Keppens, E., Baeyens, W., 2000. High resolution distribution of trace elements in the calcite shell layer of modern *Mytilus edulis*: environmental and biological controls. *Geochem. Cosmochim. Acta* 64, 997–1011. [https://doi.org/10.1016/S0016-7037\(99\)00380-4](https://doi.org/10.1016/S0016-7037(99)00380-4).
- Waeles, M., Dulaquais, G., Jolivet, A., Thébaud, J., Riso, R.D., 2013. Systematic non-conservative behavior of molybdenum in a macrotidal estuarine system (Aulne-Bay of Brest, France). *Estuar. Coast Shelf Sci.* 131, 310–318. <https://doi.org/10.1016/j.eess.2013.06.018>.
- Yamaguchi, M., Itakura, S., 1999. Nutrition and growth kinetics in nitrogen-or phosphorus-limited cultures of the noxious red tide dinoflagellate *Gymnodinium mikimotoi*. *Fish. Sci.* 65, 367–373. <https://doi.org/10.2331/fishsci.65.367>.
- Yamamoto, T., Oh, S.J., Kataoka, Y., 2004. Growth and uptake kinetics for nitrate, ammonium and phosphate by the toxic dinoflagellate *Gymnodinium catenatum* isolated from Hiroshima Bay, Japan. *Fish. Sci.* 70, 108–115. <https://doi.org/10.1111/j.1444-2906.2003.00778.x>.
- Young, J.R., 1994. Functions of coccoliths. In: Winter, A., Seisser, W.G. (Eds.), *Coccolithophores*. Cambridge Univ. Press, New York, pp. 63–82.